INFORMATION TO USERS

THIS DISSERTATION HAS BEEN MICROFILMED EXACTLY AS RECEIVED

This copy was produced from a microfiche copy of the original document. The quality of the copy is heavily dependent upon the quality of the original thesis submitted for microfilming. Every effort has been made to ensure the highest quality of reproduction possible.

PLEASE NOTE: Some pages may have indistinct print. Filmed as received.

Canadian Theses Division
Cataloguing Branch
National Library of Canada
Ottawa, Canada K1A 0N4

AVIS AUX USAGERS

LA THESE A ETE MICROFILMEE TELLE QUE NOUS L'AVONS RECUE

Cette copie a été faite à partir d'une microfiche du document original. La qualité de la copie dépend grandement de la qualité de la thèse soumise pour le microfilmage. Nous avons tout fait pour assurer une qualité supérieure de reproduction.

NOTA BENE: La qualité d'impression de certaines pages peut laisser à désirer. Microfilmée telle que nous l'avons reçue.

Division des thèses canadiennes
Direction du catalogage
Bibliothèque nationale du Canada
Ottawa, Canada K1A 0N4

THE EFFECTIVE MASS OF ELECTRONS IN THE (000) CONDUCTION BAND OF THE $GaAs_xSb_{1-x}$ ALLOY SYSTEM

by

Paul Devlin

Thesis submitted to the School of Graduate Studies in partial fulfillment of the requirements for the degree of Master of Science in Physics

Department of Physics
Faculty of Science and Engineering
University of Ottawa
Ottawa, Canada

1976

Approved for the Department of Physics

Chairman

ABSTRACT

This thesis investigates the variation of the effective mass of electrons at the bottom of the (000) conduction band for the alloy system $GaAs_xSb_{1-x}$. Infrared Faraday rotation data in the range 4 microns to 13 microns was combined with Hall effect measurements using the Van der Pauw technique. Measurements were made at room temperature and some of the samples were also studied at liquid nitrogen temperatures. The samples were cut from ingots grown using a horizontal Bridgeman technique and were n-type with a carrier concentration ranging from 10^{16} cm^{-3} to 10^{18} cm^{-3}. The Kane model for the energy bands was used to analyze the data and the variation of effective mass versus composition was found.

ACKNOWLEDGEMENTS

I would like first of all to thank Dr. Woolley for his suggestion of the topic of study and for his advice during the course of the project. I am also very appreciative of the innumerable occasions on which I have been aided by the staff and the students of the Physics department. A special thanks is due to Dr. Stanley Rosenbaum for supplying the $GaAs_xSb_{1-x}$ ingots used for this work and to Mr. R.G. Goodchild for x-raying the samples.

I am very grateful for the financial assistance, that I received from the National Research Council.

Finally, I wish to express my sincere gratitude to my parents for their encouragement and to my wife, Lise, for typing this thesis and providing an atmosphere conducive for achievement.

TABLE OF CONTENTS

LIST OF FIGURES

LIST OF TABLES

I INTRODUCTION

1.1 ORIGIN OF THE PROJECT

During the past few years a great deal of research has been aimed at analyzing the properties of the ternary alloys formed from the III-V compounds InSb, InAs, GaSb and GaAs. Previous workers (66T1, 69A1, 71T1) have found the bottom of the conduction band effective mass as a function of composition. Using four experimental methods: cyclotron resonance, infrared reflectance, magneto-thermoelectric power and Faraday rotation, all possible combinations of these compounds with the exception of $GaAs_xSb_{1-x}$ have been studied.* The scope of this thesis then, is to provide the values of $m^*_{oo}(x)$ for this system. Since the $GaAs_xSb_{1-x}$ ingots that were available at the time that specimens were prepared tended to have p-type GaAs rich ends, only the GaSb end of these ingots was used.

1.2 HISTORICAL BACKGROUND

The historical background to the work done in this thesis would not be complete without mentioning Michael Faraday (1791-1869) who made many pivotal discoveries in physics and chemistry. One such discovery was the effect which now bares his name - the Faraday effect. This effect is the rotation of the plane of polarization of plane polarized light as it propagates through a medium in the presence of a longitudinal magnetic field. His diary (B1) states that on the 13'th of September in 1845 after having tried a number of configurations using his electromagnets and a glass block that "when contrary magnetic poles were on the same side there was an effect produced on the

*Since this work was written there has been some results published on this alloy system (Filion, Fortin C.J.P. 52, 743, 1974).

polarized ray." His experimental set-up is shown in Fig.1.1.

Earlier, in 1825, Fresnel had shown that natural optical rotation the plane polarized wave could be considered as right and left circularly polarized waves travelling through the medium at different velocities. Thus the rotation of the plane of polarization for light passing through a material of length ℓ is given by the angle

$$\theta = \frac{\omega\ell}{2}(n_- - n_+)$$

where n_- and n_+ are the refractive indices of the negative and positive components of the radiation and c is the velocity of light (SI).

An explanation of this effect, in terms of electron motion, was not made until 1897 when Becquerel gave the relationship between the Faraday effect and the dispersion as

$$\theta = \ell\omega\omega_L\frac{dn}{d\omega}$$

where $\omega_L = \frac{eB}{2m}$ is the Larmor frequency, e is the magnitude of the charge of the electron and m is the mass of the electron. The two components then have an angular frequency $\omega - \omega_L$ and $\omega + \omega_L$.

During this same period, in 1879, the American physicist Edwin Hall (1855-1938) discovered the Hall effect. This effect is the potential difference which appears across a conductor when a magnetic field is applied to the conductor perpendicular to the direction of the current flow.

Both the Faraday effect and the Hall effect have proven to

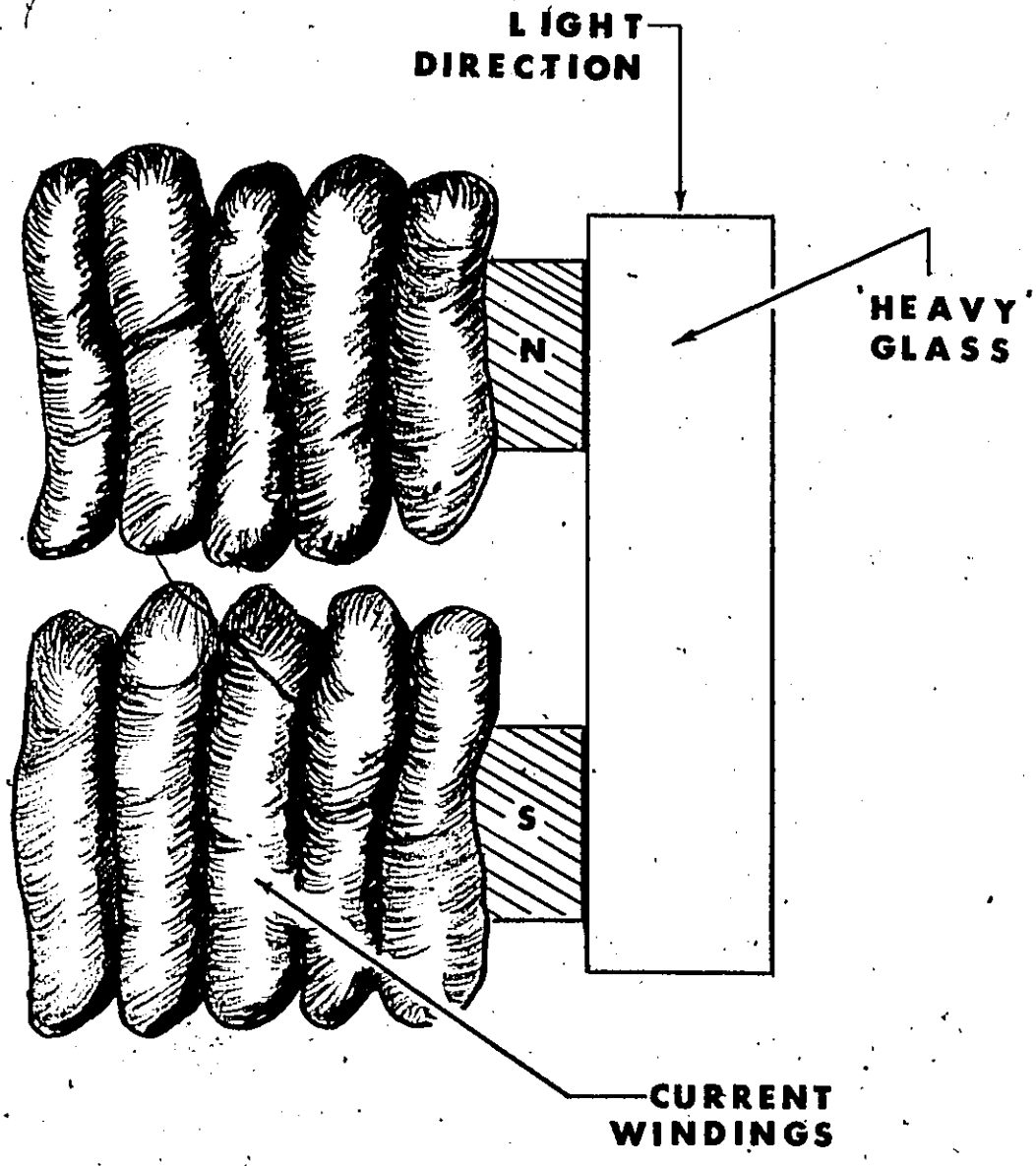

Fig. 1.1 Faraday's experimental set-up

be very useful methods of analyzing the energy band structure of semiconductors.

The study of semiconducting crystals goes back to the invention of copper oxide rectifiers in the 1920's. The behaviour of the copper oxide rectifiers could never be completely understood because of the unknown way in which their operation depended on the manner in which the oxide was prepared. However two key events occurred in the late 1940's which loosened a flood of discoveries and these were the discovery of the transistor action by Brattain, Bardeen and Shockley and secondly the development of the zone refining process for growth of high purity Si and Ge crystals by Pfann(P1). In the early 1950's Welker (52W1, 56W1, 56W2) and others indicated that the III-V compounds had semiconducting properties similar to those of Si and Ge. Not only the compounds but also the mixed crystal systems were also investigated and found to be semiconducting. $InAs_xP_{1-x}$ was one of the first such systems investigated. It was observed that by alloying two semiconductors of different characteristics, one could generate a system with properties ranging between the extremes. The ternary alloy $GaAs_xP_{1-x}$ is a good example of the commercial exploitation of this principle. This system, which was one of the first to be investigated, is now used to fabricate light emitting diodes whose wavelength of radiation is dependent on the principal energy gap. As a result, for $x = 1.0$ the radiation is in the infrared, for $x = 0.6$ the radiation is red and finally for $x = 0.0$ the radiation is green.

Besides the aspect of device application, the other reason that alloy study is important is the knowledge gained about the energy band structure. By alloying different III-V compounds and by measuring the principal energy gap (Eg) or the effective mass as a function of the composition we gain an insight into the band structure. If two compounds with similar band structures are alloyed, then we expect to see a smooth variation with composition. If on the other hand the conduction and valence bands are of different forms, we might find an abrupt change of slope in the dependence of Eg at some intermediate composition. This result appears in the $GaAs_xP_{1-x}$ system for Eg versus composition. A kink in the curve arises, because in GaAs there is a direct transition where as in GaP the transition is indirect.

1.3 ELEMENTARY BAND THEORY

The energy bands of semiconductors arise from the individual electronic states of the atom. The isolated atom has discrete energy levels but as the atoms are brought closer together and the internuclear spacing decreases, the electronic energy levels spread into a band see Fig. 1.2. The overlapping of the valence electron orbits corresponds to an interatomic coupling which causes each separate, allowed valence electron energy level to split up into a band of allowed energy levels characteristic of the crystal. Electrons in the states nearest the nuclei interact with the fields of

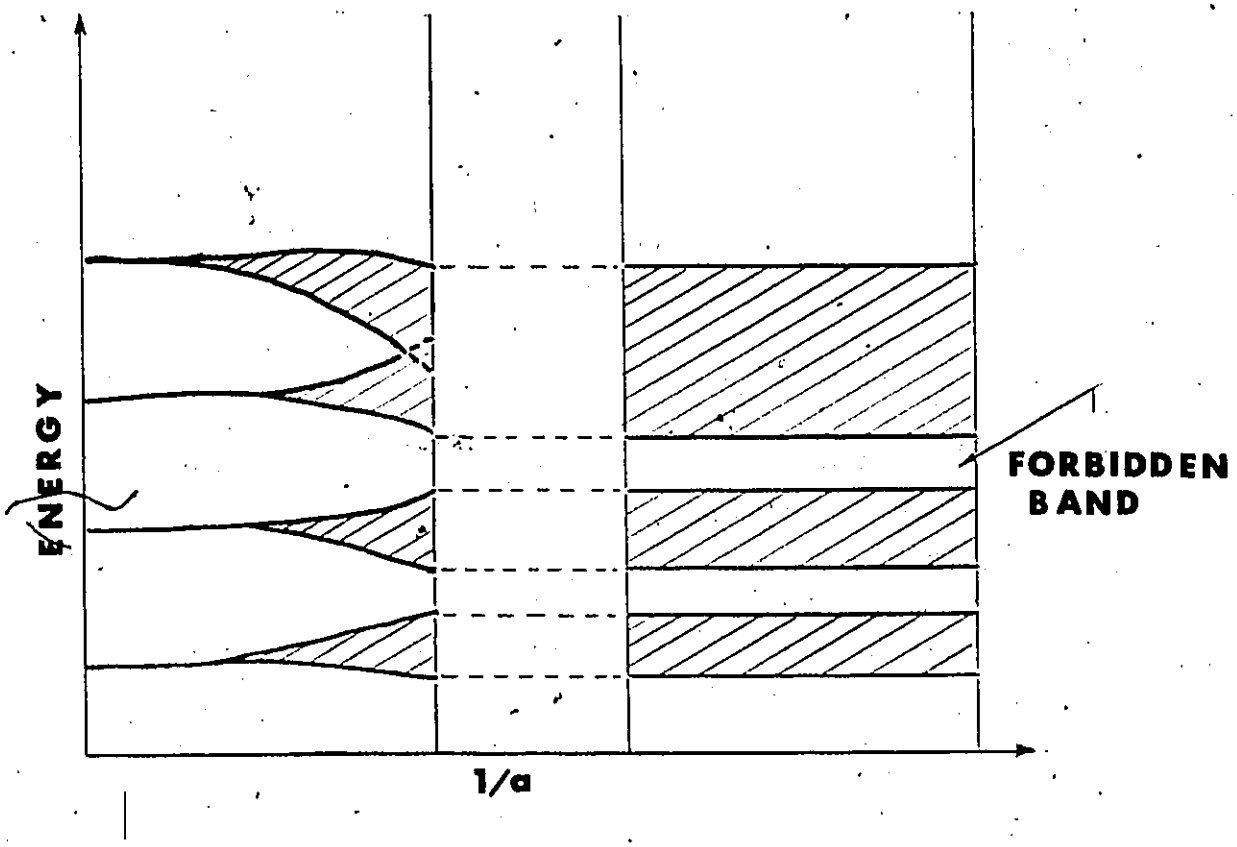

Fig. 1.2 The spreading of energy levels into bands

neighbouring nuclei to a lesser extent hence the bands they produce will be narrower than those formed by valence electrons. The resultant band structure determines whether the solid is an insulator, metal or semiconductor (E1, P2). The band structure so produced also contains regions where electrons are not permitted and these are called the forbidden bands. Pure semiconductors and insulators are similar since at 0^{0}K their energy bands are either completely full or completely empty and so their electrons cannot change their net energy state without traversing the forbidden gap. The difference between them lies in the magnitude of their forbidden gap; it is much larger in the case of the insulator. In a metal the bands are never completely full so little energy is required to change the state of the electrons (I1).

The mathematical analysis of band structure in a solid is simplified if we use a single electron approximation assuming this electron to belong to the whole lattice. The potential that this electron then experiences is that due to the nuclei in the lattice plus the charge distribution of the other electrons. As a result, the electron is subjected to a periodic potential. The basic equation used to analyze this problem is the Schrodinger wave equation introduced by the Austrian physicist Erwin Schrodinger in 1926. This equation which is applicable to the motion of particles in any field of forces was derived from the work done by de Broglie (B1). For one dimension the equation is

$$\Delta^2\Psi + \frac{2m}{\hbar^2}(E-V(x))\Psi(x) = 0$$

When the potential function V(x) is periodic so that V(x+a) = V(x) then it has solutions of the form $\Psi_K(r) = e^{ik.r}\, U_K(r)$ for three dimensions. This result is known to mathematicians as Floquet's theorem.

The Block function, $U_K(r)$, is a periodic function with the periodicity of the lattice. The functions $e^{ik.r}$ represent plane waves and have momentum $p = \hbar k$. The plane waves would be the solution of the Schrodinger wave equation in a constant potential. This Bloch wave represents a flux of particles since the K vector is related to the momentum of a wave by the de Broglie relation. The particles move uniformly through an ideal lattice completely unhindered by the atoms (P1).

The energy gap can be thought of as arising from the Bragg reflection of electron waves at certain values of k for which constructive interference occurs.

In the simple cubic crystal, the first planes off which diffraction can occur are the close packed [100] planes since the distance between these planes is larger than that for any other. Bragg's law for the [100] planes is

$$n\lambda = 2d \cos\theta \text{ or } \pi n = \vec{k}\cdot\vec{d}$$

For diffraction of the lowest order (n = 1) there are 6 equivalent diffracting planes in k space corresponding to the six [100] planes.

From this argument we can see that at certain energies for

which $k = \pm \frac{n\pi}{a}$ where $n = 1,2,3,\cdots$ and a is the lattice parameter, there is no Bloch function solutions for the wave equation. On comparing, in one dimension, the E vs k curves for free electrons and those subject to a periodic potential we see that they are similar except for the presence of forbidden regions in the latter case. In three dimensional K space the discontinuities enclose a volume, the first of which is called the first Brillouin zone. From the previous analysis of Bragg reflection in a simple cubic crystal we see that in this case the first Brillouin zone is simply a cube. For a face centered cubic crystal the Brillouin zone is truncated octahedron.

Up until now we have considered what is known as the extended zone scheme, however if we encounter a Bloch function with K outside the first zone we may always find a suitable reciprocal lattice vector G´ such that $k = k' - G'$ lies within the first Brillouin zone. This is a result of the periodicity of the Bloch functions in the crystal lattice. As a result we can construct a reduced zone scheme in which we find different energies at the same value of the wave vector. Each different energy characterizes a different band. In three dimensions the energy band scheme is drawn from the (000) point along the directions possessing extrema in the energy variation. These extrema usually lie in the <111> and the <100> direction in cubic semiconductors. This reduced zone scheme is shown for GaSb

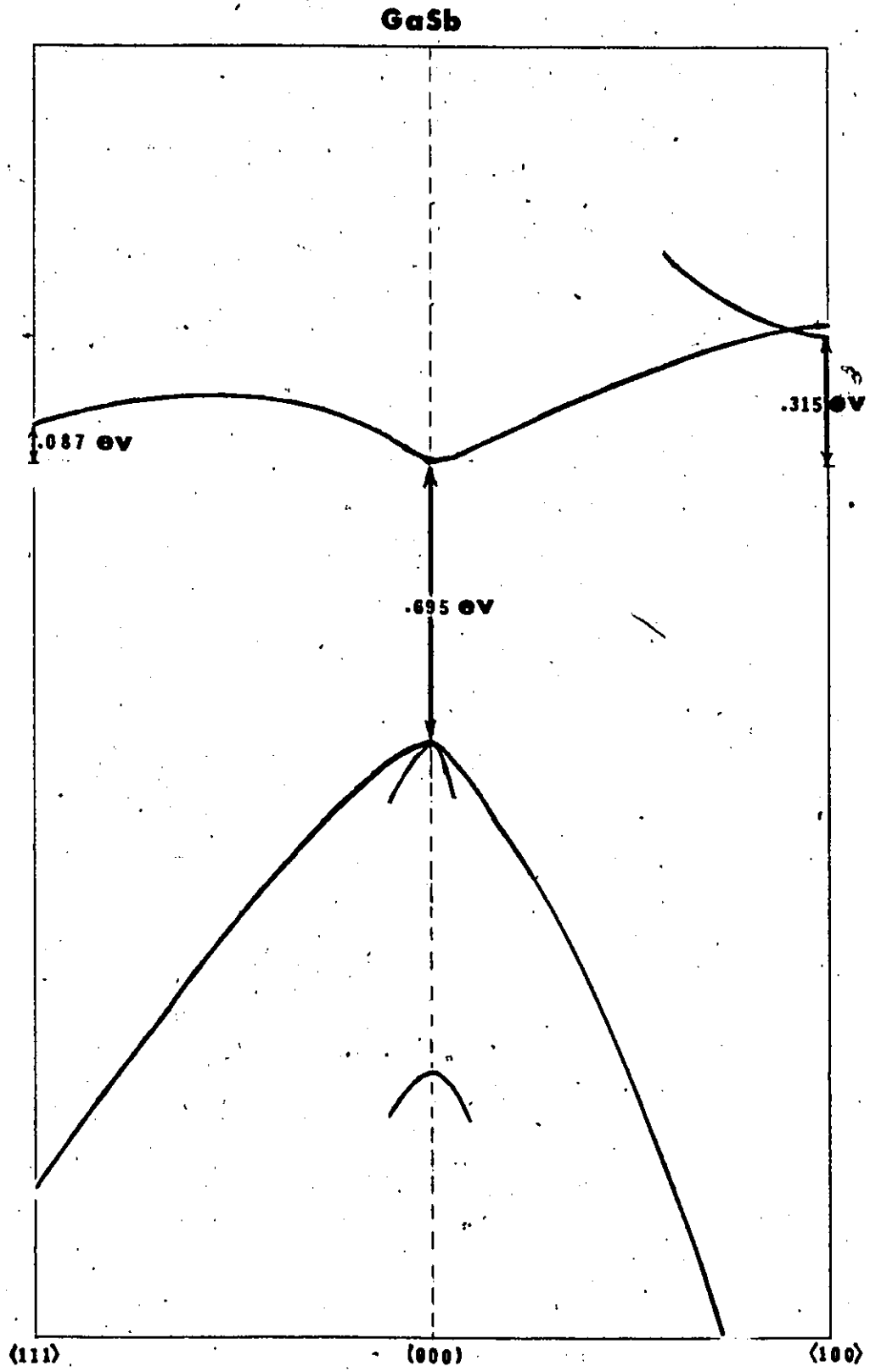

Fig. 1.3 The energy band structure at GaSb at room temperature

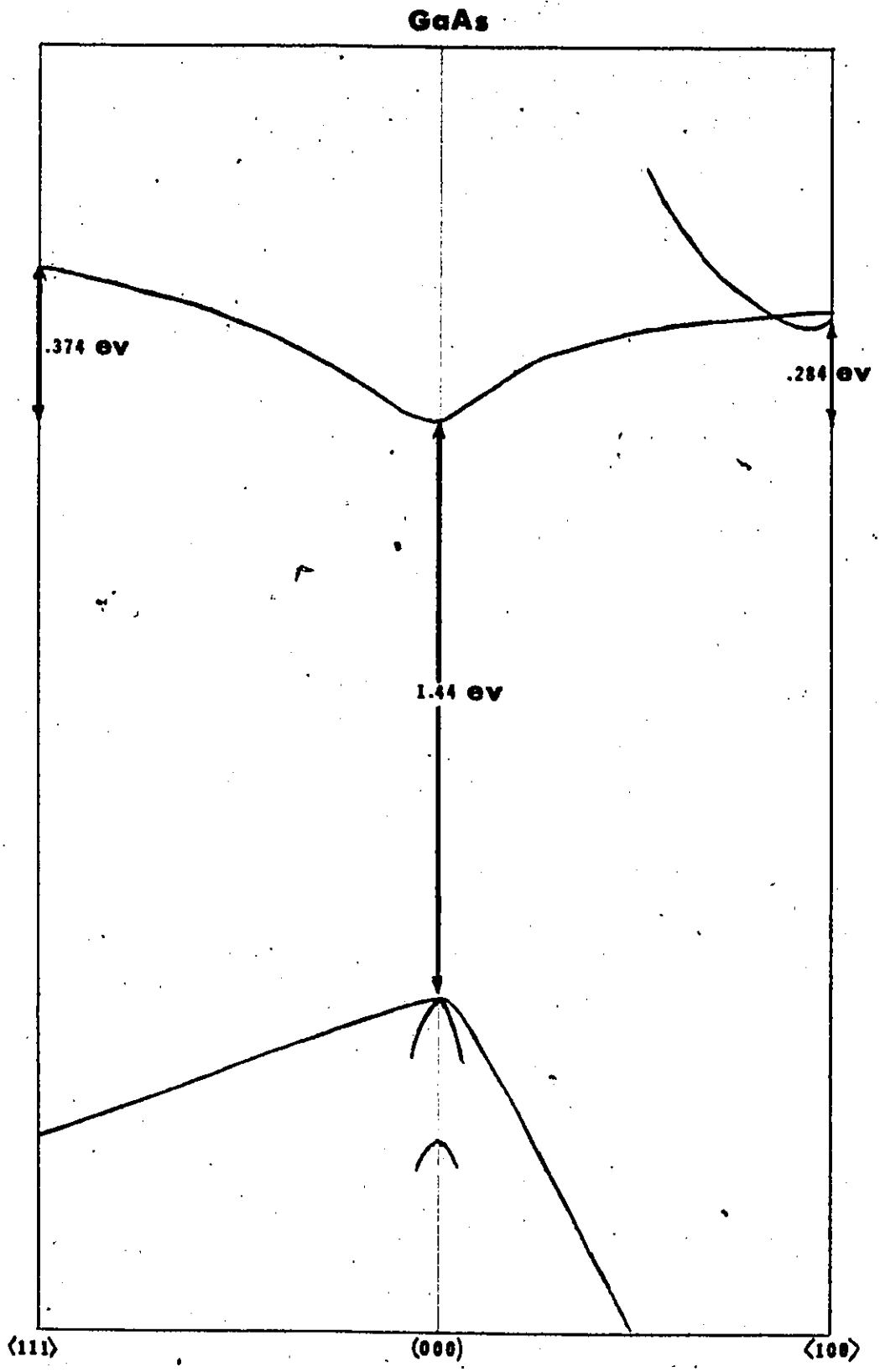

Fig. 1.4 The energy band structure of GaAs at room temperature.

and GaAs in Fig. 1.3 and Fig. 1.4.

1.4. CRYSTALLOGRAPHY

The III-V compounds crystallize into the zincblende struture (ZnS). This structure can be pictured verbally if we consider the lattice to be formed from two interpenetrating face centered cubic sublattices displaced from one another by a quarter of the distance along the body diagonal. Each atom is then at the center of a tetrahedron with four opposite atoms at its vertices: (see Fig. 1.5). In the case of $GaAs_xSb_{1-x}$ the tetravalent atoms occupy one f.c.c. lattice and the pentavalent atoms occupy the other.

While the structure of the compounds is fairly clear the question that arises is what is the structure of an alloy of two compounds? The simplest case is that of a ternary alloy i.e. one in which one of the component atoms is common to both compounds. In the case of $GaAs_xSb_{1-x}$, Ga is the common element. Experiments show that this ternary alloy can be pictured as a continuous zincblende phase in which the common element occupies all the points of one lattice and the other atoms are randomly distributed on the other lattice. Although the macroscopic variation is shown quite accurately by X-ray films, the variation on the microscopic scale is not known.

There have been different simplified models (B2) proposed for analysis of disordered alloys, the simplest of which is the rigid band model (Mott and Jones 1936, 1958). The potential for the alloy is constructed from the periodic potential of the matrix atoms and is

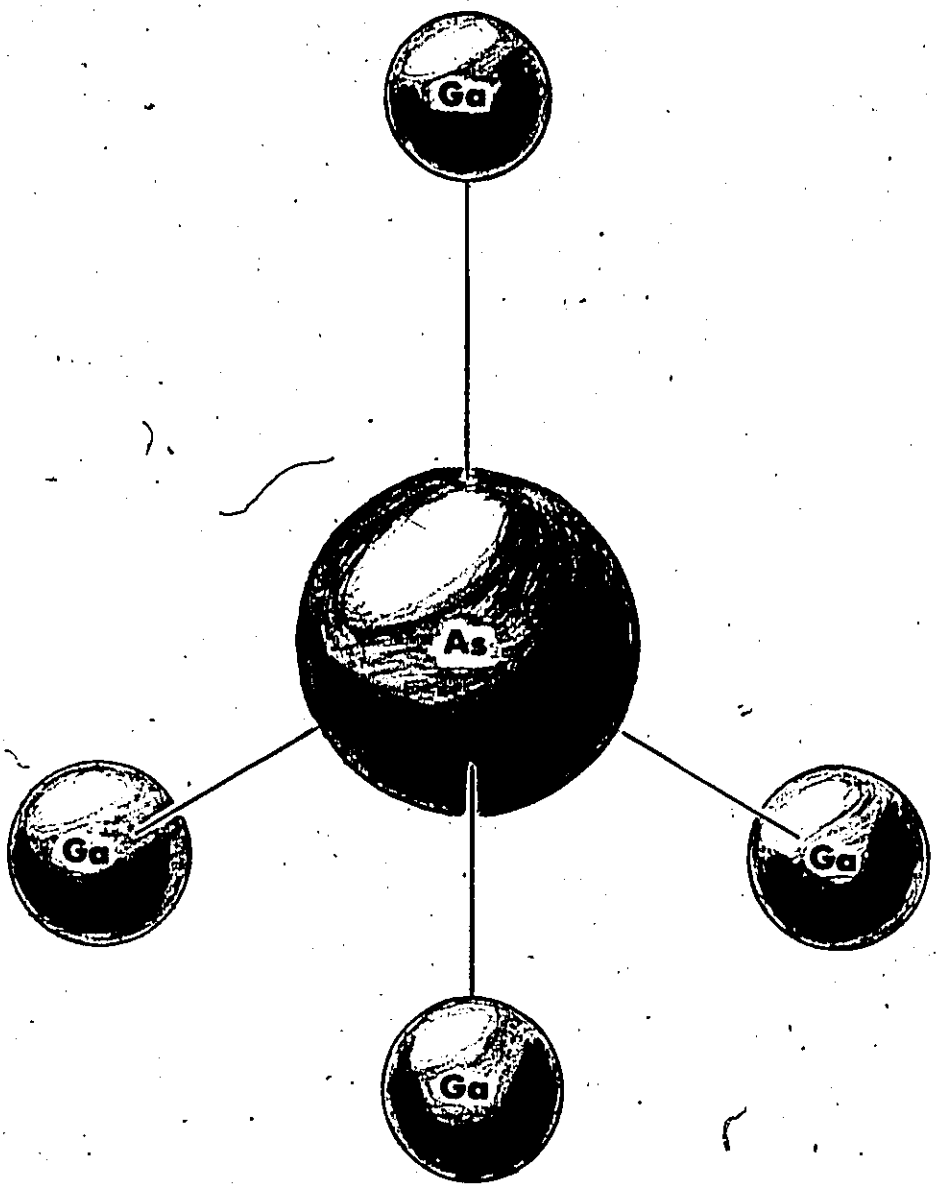

Fig. 1.5 The tetrahedral arrangement of the atoms in GaAs.

perturbed by the potential due to the different fields of the solvent and solute atoms.

However the application of the rigid band approximation can be justified only when the concentration of solvent greatly exceeds the concentration of the solute. The next development in the theory of disordered alloys was a model suitable for any concentration of the alloy constituents (Nordheim 1931, Parmenter 1955, Schoen 1969). This model assumes the alloy electrons behave like electrons in a hypothetical ordered system, where the crystal potential is an average of the potentials of the components weighted according to their concentration. The potential of the lattice consists of two parts - a periodic part and an aperiodic part where the periodic potential varies linearly with alloy composition. The periodic part is the average alloy potential, for a specific composition, taken over all possible configurations of the atoms and the aperiodic part is the deviation from the average. The periodicity can be seen to arise from the fact that the atoms occupy the zincblende structure. The aperiodic part arises from the random distribution of the non-common atoms. Nordheim proposed a virtual crystal model in which the periodic potential is used to determine the band structure of this virtual crystal and the effect of the aperiodic part is then treated as a perturbation. Considering the virtual crystal model, a smooth variation of the various parameters is predicted, and Parmenter has

predicted a x(1-x) type variation in parameters when second order perturbation is considered.

1.5 CRYSTAL GROWTH

Commercial crystal pullers are now available capable of producing single crystals of III-V compounds weighing several kilograms. GaAs and GaP are presently needed in large quantities to supply a large L.E.D. market. Problems that in the early stages of research were quite serious such as high melting points, toxity of the pentavalent atoms and the high vapour pressure of arsenic, have largely been overcome.

As mentioned previously the samples used in this thesis were cut form ingots grown using a horizontal Bridgman technique (25B1). This technique consists of slowly pulling an evacuated ampoule containing the ternary melt from a hot zone in which the alloy is molten through a sharp temperature gradient to a cool zone. The ampoule is left a sufficiently long time in the hot zone so that mixing is complete before passing through the gradient. The resultant ingot has a composition which varies with the length of the ingot as shown in Fig. 1.6. The first part to solidify is the high melting point component; in the present case the GaAs rich material solidifies first. As the ingot is removed from the hot zone the melt becomes richer in the lower melting point component.

Not all combinations of III-V compounds give completely miscible alloys over the whole range of x. The extent of solid

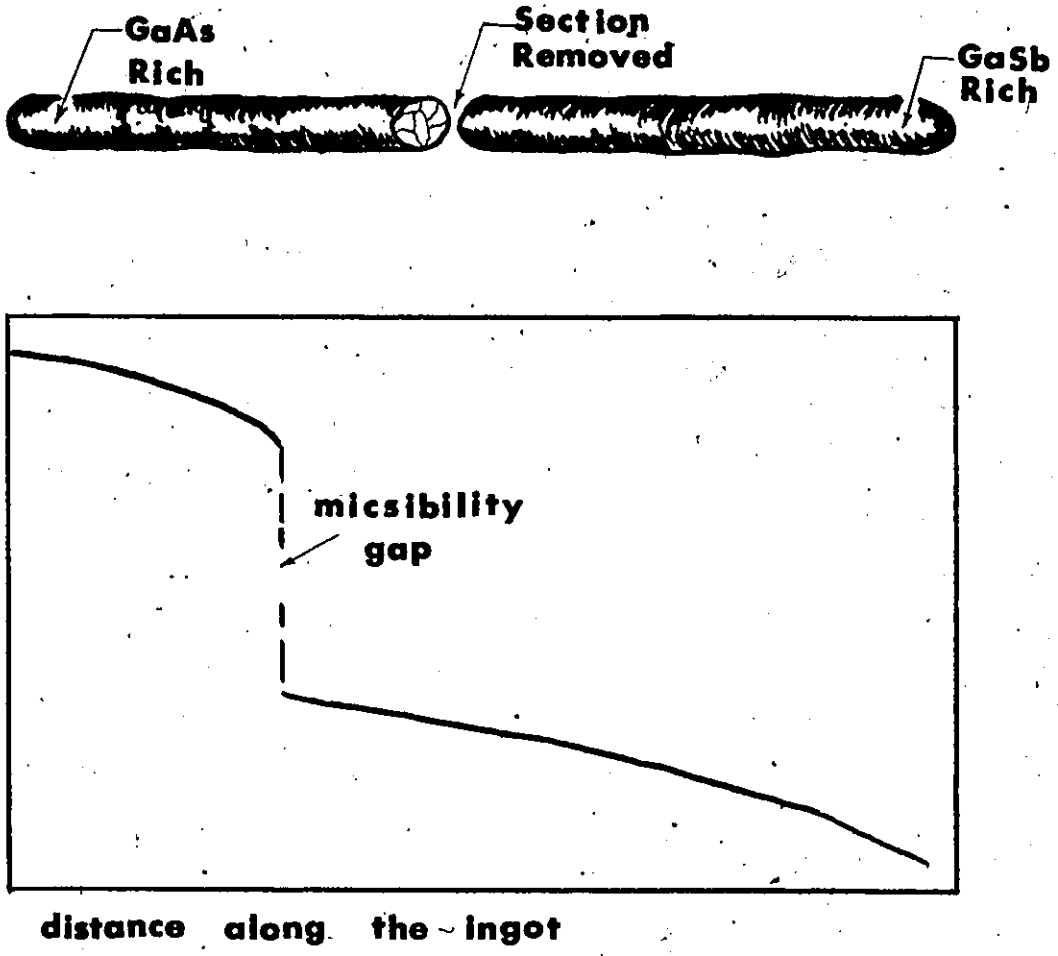

Fig. 1.6 The variation of composition along the length of the ingot.

solubility is generally smaller the larger the size difference between the atoms. A rule for this, first stated by the metallurgist Hume-Rothery, describes the behaviour found for many alloy systems. Large terminal solid solubility is not possible if the two atoms differ in size by much more than 15 percent. The rule must be applied with care because a favourable size ratio is a necessary, but not sufficient reason for large solubility. In the $GaAs_xSb_{1-x}$ system there is a miscibility gap from $.38 \leq x \leq .61$ (73 G1).

This method of growing bulk samples is ideal for the study of alloys since the resultant ingot has a varying composition from one extreme to another. The material is usually homogeneous since several weeks are spent pulling it through the step - thus giving the solid a slow growth schedule and also time to anneal at a temperature very close to the solidus temperature. The one disadvantage is that the resultant material is polycrystalline and ideally we would like to work with single crystals.

Possibly future workers who will investigate the alloys in greater detail will take advantage of vapour or liquid phase epitaxial methods capable of growing several hundred microns of single crystal material at various compositions and doping levels on single crystal substrates.

II THEORY

2.1 SIMPLE THEORY

The initial sections of the theory developed in this chapter are taken from numerous texts to which references have been made. The latter sections dealing with conductivity and Boltzmann theory comes primarily from theory developed by C.R. Pidgeon (P5) and Eric Van Tongerloo (T1) in their doctoral theses.

The aim of this section of the theory is to relate the net rotation, θ, experienced by the linearly polarized radiation, to the refractive indices of the radiation within the semiconducting crystal. A chronological ordering is used starting with the early results of Fresnel. Several sections of the theory involve long algebraic development and for the sake of readability those sections are left to the appendices, or references are given to other sources. The most important result of this theory is the relation between the rotation and the refractive index because this result is used at further stages in the development. However in this same subsection I shall also introduce Drude's theory for the equation of motion of an electron in an electric and magnetic field. By so doing we are able to relate the rotation to more basic energy band parameters, such as the effective mass. From this result we can obtain certain information about the energy band as long as certain considerations are kept in mind. In the development several approximations are employed and an effort has been made to justify their use.

ii RESULTS OF EARLY EXPERIMENTERS

(a) Fresnel, Becquerel

The explanation of optical rotation was given by Fresnel (1825) who showed that when a plane polarized vibration enters a plate of axis cut quartz the vibration is resolved into two equal circular vibrations rotating in opposite directions. These two circular vibrations travel through the plate at unequal velocities and therefore emerge with a difference in angular phase. Two circular vibrations of equal amplitude and period but rotating in opposite directions when acting together are equivalent to a rectilinear vibration (01).

The explanation (P3) of the natural rotation in active substances which Fresnel gave will do for magnetic rotation provided that it can be shown that the refractive index of a medium in a magnetic field for circularly polarized light depends on the direction of the revolution.

This problem was attacked experimentally by Righi and Becquerel independently and both investigators found that the interference fringes formed by two streams of circularly polarized light, one of which has traversed a block of glass placed between the poles of a magnet, were displaced when the magnetic field was formed. The direction of displacement depended on whether right or left-handed circular light was used, which showed that the effect

of the field was to increase the refractive index for one type of vibration and diminish it for the other.

Becquerel's result is summarized in an equation named after him

$$\theta = \frac{\ell\omega\omega}{2} c \frac{dn}{d\omega} \qquad (2.1)$$

In this equation θ is the angular rotation, ω is the angular frequency of the radiation passing through the sample, η is the refractive index of the material and ω_c is the cyclotron frequency. The cyclotron frequency, whose value is

$$\frac{eB}{m}$$

introduces the magnetic field value to the equation.

(b) The relation between θ and the refractive index

If we consider a plane polarized wave as consisting of the two circularly polarized components then the application of a magnetic field along the direction of propagation of the radiation will subject each component to a different refractive index. We may consider clockwise rotation from the reference of the source as positive and use the subscript "+" to label such rotations. Counter clockwise rotations will be labled "-" and so using this format we have η_+ representing the refractive index for clockwise rotation and η_- representing the refractive index for counter clockwise rotation.

With this model in mind and using basic physical formulas

for refractive index and velocity we obtain the following expression for rotation:

$$\theta = \frac{t\pi}{\lambda}(n_- - n_+) \qquad (2.2)$$

*See appendix A

The rotation is in radians, t is the thickness of the sample and λ is the wavelength of the radiation in a vacuum. We can see that if $n_+ \simeq n_- \simeq n$ then $n_-^2 - n_+^2 = (n_- - n_+)(n_- + n_+) \simeq 2n(n_- - n_+)$

Substituting this value into equation (2.2) we obtain

$$\theta = \frac{t\pi}{2\lambda n}(n_-^2 - n_+^2) \qquad (2.3)$$

It is this form of the expression for rotation that is required in the more advanced theory that is developed later.

iii DRUDE THEORY

(a) Equation of Motion for an Electron

In order to relate the angular rotation of the radiation to the effective mass of the electrons, we shall now study Drude's theory of dispersion. If we consider an electron to be displaced by a force which instantly ceases, then the electron is drawn back by the elastic force of restitution and vibrates with a definite period depending on its mass, charge and the force of restitution. Forces akin to friction damp this vibration and eventually bring the electron to rest.

With the magnetic induction $\vec{B}$ along the z axis the classical equation of motion of an electron (02) driven by an applied field

$E_o e^{\pm i\omega t}$ is $m^* \frac{d^2s}{dt^2} + gm^* \frac{ds}{dt} - iBe \frac{ds}{dt} = eE_o e^{\pm i\omega t}$ (2.4)

where $s = x + iy$ is the complex displacement of the electron and the $\pm i\omega t$ exponents describe two contrarotating circularly polarized waves. The quantity m^* is the electron effective mass and e the electronic charge magnitude. The $gm^* \frac{ds}{dt}$ term represents viscous damping and provides for an energy loss mechanism arising from various scattering mechanisms in a solid. The nucleus is assumed to have infinite mass, otherwise the reduced mass should have been used. The small force $-e\vec{v} \times \vec{B}$ arising from the interaction of the electron with the magnetic field of the radiation has been neglected since $v \ll c$.

The solution to this differential equation is a complex amplitude

$$s = \frac{(e/m^*) E_o e^{\pm i\omega t}}{\omega(-\omega \pm \omega_c \pm ig)} \qquad (2.5)$$

From this expression for the complex amplitude we may now obtain a value for the dielectric constant.

(b) The Expression for Rotation

The electric field forces cause positive and negative charges to move in opposite directions causing a dipole moment, the direction of which coincides with the electric field (P 4). In a first approximation, the value of the dipole moment may be taken to

be proportional to the field. The polarization is $P = Nes$ where e and s are already defined and where N is the number of electrons per unit volume. The dielectric constant ε is given by the expression $\varepsilon_{\pm} = (\eta_{\pm} - i\kappa_{\pm})^2 = 1 - \frac{Ne^2/(m^*\omega\varepsilon_o)}{(-\omega \pm \omega_c \pm ig)}$ where $g = \frac{1}{\tau}$ (2.6)

This relation equates the optical constants of the material to the effective mass, electronic charge, etc. Here η is the refractive index κ is the extinction coefficient. We can now relate the rotation of the radiation to the effective mass, etc. by using this equation. To do this we assume that the extinction coefficient is small compared to the refractive index i.e. that $\eta^2 >> \kappa^2$ and also that $\omega^2 >> \omega_c^2$ and $\omega\tau >> 1$. After manipulating equation (2.6) and then substituting into equation (2.3) we obtain

$$\theta = \frac{BNe^3t}{2\eta c\varepsilon_o m_{ic}^{*2}\omega^2} \qquad (2.7)$$

appendix B

We immediately see that the rotation is proportional to $\frac{1}{m_{ic}^{*2}}$, so it becomes apparent that the Faraday rotation data in conjunction with the carrier concentration can be used to evaluate the effective electronic mass. The effective mass value that appears in this equation is the cyclotron effective mass, which is equal to $\frac{1}{k}\frac{dE}{dk}$.

iv CALCULATIONS BASED ON THIS THEORY

Since we now have a relation between the rotation and the

cyclotron effective mass, we may now make some limited calculations. The first requirement is that the semiconductor have a high degeneracy; by which we mean that the Fermi energy is greater than 4KT above the conduction band minimum. The second requirement is that the surfaces of constant energy be spherical. With these conditions it has been shown (58 S1) that the cyclotron effective mass is interpreted as

$$\frac{1}{m^*_{ic}} = \frac{1}{\hbar^2}\frac{1}{k_f}\frac{dE}{dk}\Big]_f \qquad (2.8)$$

where the subscript i = 0, 1 or 2 signifies (000), <III> and <100> conduction bands respectively. The subscript c reminds us it is the cyclotron effective mass and the f implies that the slope of the E vs k curve is found at the Fermi level. The basic procedure for deriving the shape of the energy band is fairly straightforward. If we again consider equation (2.7)

$$\theta = \frac{BNe^3 t}{2nc\epsilon_o m^{*2}_{ic}\omega^2}$$

it becomes evident that after performing a Faraday rotation experiment and a Van der Pauw measurement then all values except the refractive index n and m^*_{ic}, the cyclotron effective mass, are known. The refractive index values for an alloy in general are not available although some III-V alloy systems have had results tabulated (67 C1). These results show a linear variation from x = 0.0 to x = 1.0. Based on these results and assuming a similiar linear relationship for the $GaAs_xSb_{1-x}$ system, we may evaluate the refractive

index by finding the values of the compounds and then assuming a linear variation. An inspection of equation (2.6) however shows that the refractive index is a function of the concentration of free carriers, so a correction must be applied for those samples which are highly doped.

At this juncture we know all values except the cyclotron effective mass which we can now proceed to solve for. Once we have obtained the value for effective mass we can solve for the slope of the conduction band at the Fermi level. This solution also requires a knowledge of k_f , the Fermi radius (59 Sl)

$$k_f^3 = 3\pi^2 N$$

v Justification of the Approximations

The analysis of this section of the theory resulted in equations that were derived using three approximations

(a) . $\eta^2 >> \kappa^2$

Verbally this approximation states that the absorption of the radiation within the sample is small. Absorption is not usually measured in terms of the extinction coefficient κ, but rather in terms of the absorption coefficient α which appears in the expression $I = Ioe^{-\alpha x}$ where Io is the incident intensity. The relationship which equates the extinction coefficient to the absorption coefficient is $\kappa = \frac{\alpha\lambda}{4\pi}$ where λ is the wavelengh in a vacuum.

Taking absorption coefficient values for GaAs as typical, I found

that for $\alpha = 300.\ cm^{-1}$ at 0.9μ and $\alpha = 21\ cm^{-1}$ at 19μ the values of $k = 0.002$ and 0.003 respectively. The value of the refractive index is greater than 3.0 so the approximation $n^2 >> \kappa^2$ is valid.

(b) $\omega^2 >> \omega_c^2$, $\omega >> \tau^{-1}$

The approximation $\omega^2 >> \omega_c^2$ states that the square of the angular frequency of the radiation used to obtain the Faraday rotation is larger than the square of the cyclotron resonance frequency. Since $\omega_c = \frac{eH}{m^* c}$ we find by substituting into this expression approximate values, that $\omega_c \approx 10^{13}$. Values of angular frequency that were used in this experiment were generally all greater than 20×10^{13}. It is safe to say then that $\omega^2 >> \omega_c^2$ and in a similar way by taking approximately known values of τ it can be shown that $\omega\tau >> 1$.*

2.2 CONDUCTIVITY THEORY

i Introduction

The theory (T1) that is developed in this section has the basic goal of expressing the rotation in terms of the conductivity of the specimen. To do this we first establish a relationship between the refractive index and the conductivity by using Maxwell's equations. The equation is solved for the refractive index and this is substituted into equation (2.3). Certain approximations are used during the development to obtain a simplified result.

* Note that the upper limit for ω is given by $\hbar\omega < E_g$, where E_g is the energy gap.

ii The Relation between the Refractive Index and the Conductivity

If we manipulate Maxwell's field equation for a conducting medium we obtain the wave equation

$$\nabla^2 \vec{E} - \mu \frac{\partial \vec{J}}{\partial t} - \mu\varepsilon \frac{\partial^2 \vec{E}}{\partial t^2} = 0 \qquad (2.9)$$

where $\vec{E}$ is the electric field vector and $\vec{J}$ is the current density. The values μ and ε are the permeability and the dielectric constant respectively. This expression is arrived at by taking the curl of the expression

$$\nabla x \vec{E} = - \mu \frac{\partial \vec{H}}{\partial t} \qquad (2.10)$$

and substituting $\nabla x \vec{H} = \vec{J} + \varepsilon \frac{\partial \vec{E}}{\partial t}$ into the resulting equation.

Abeles and Meiboom (54 A1) have shown that for cubic crystals in the presence of a static magnetic field $\vec{H}$ the component of the current density may be written to second order as

$$J_i = \Sigma_{ij} E_j + \Sigma_{ijk} H_k E_j \qquad (2.11)$$

where $\Sigma_{ij} = \sigma \delta_{ij}$, $\Sigma_{ijk} = \sigma' \varepsilon_{ijk}$ and δ_{ij} is the Kronecker delta and ε_{ijk} is the substitution tensor. Here σ and σ' are both complex conductivities i.e.

$$\sigma = \sigma_r + i\sigma_i \quad , \quad \sigma' = \sigma'_r + i\sigma'_i \; .$$

The subscripts r and i refer to real or imaginary quantities.

Now we substitute the value for the current density back

into the wave equation and let $E\pm = Eo\pm \exp \frac{i\omega}{c}(N\pm r + ct)$ represent the electric field of a plane polarized wave. The x and y components of the resulting equation are

$$\frac{\partial^2 E_x}{\partial x^2} - \mu\sigma\frac{\partial E_x}{\partial t} - \mu\sigma'\frac{\partial E_y}{\partial t} H_z - \mu\varepsilon\frac{\partial^2 E_x}{\partial t^2} = 0 \qquad (2.12)$$

$$\frac{\partial^2 E_y}{\partial y^2} - \mu\sigma\frac{\partial E_y}{\partial t} + \mu\sigma'\frac{\partial E_x}{\partial t} H_z - \mu\varepsilon\frac{\partial^2 E_y}{\partial t^2} = 0 \qquad (2.13)$$

If we multiply (2.13) by $\pm i$ and add to (2.12) we obtain

$$\frac{\partial^2 E_\pm}{\partial r^2} - \mu\sigma\frac{\partial E_\pm}{\partial t} \pm i\mu\sigma'\frac{\partial E}{\partial t} H_z - \mu\varepsilon\frac{\partial^2 E_\pm}{\partial t^2} = 0 \qquad (2.14)$$

Substituting the values for σ', σ and $E\pm$ and solving for the square of the complex refractive index $N_\pm^2$ we obtain

$$N_\pm^2 = \mu c^2\left[\varepsilon + \frac{\sigma_i}{\omega} \mp \frac{\sigma' H_z}{\omega} - i\left(\frac{\sigma_r}{\omega} \pm \frac{\sigma_i H_z}{\omega}\right)\right] \qquad (2.15)$$

where $N_\pm = n_\pm - i\kappa_\pm$. The real and imaginary value of the complex refractive index may be determined by using the following mathematical indentities:

If A is a complex number then

$$(\mathrm{Re}(A))^2 = \frac{1}{2}\left[\mathrm{Re}(A^2) + \sqrt{(\mathrm{Re}(A^2))^2 + (\mathrm{Im}(A^2))^2}\right]$$

$$(\mathrm{Im}(A))^2 = \frac{1}{2}\left[-\mathrm{Re}(A^2) + \sqrt{(\mathrm{Im}(A^2))^2 + (-\mathrm{Re}(A^2))^2}\right]$$

The values of $\eta_\pm^2$ and $\kappa_\pm^2$ that result from using these identities are

$$\eta_\pm^2 = \frac{c^2\mu}{2}\left[\varepsilon + \frac{\sigma_i}{\omega} \mp \frac{H_z}{\omega}\sigma_r' + \sqrt{(\varepsilon + \frac{\sigma_i}{\omega} \mp \frac{H_z\sigma_r'}{\omega})^2 + (\frac{\sigma_r}{\omega} \pm \frac{H_z\sigma_i'}{\omega})^2}\right]$$

$$\kappa_\pm^2 = \frac{c^2\mu}{2}\left[-\varepsilon - \frac{\sigma_i}{\omega} \pm \frac{H_z\sigma_r'}{\omega} + \sqrt{(\varepsilon + \frac{\sigma_i}{\omega} \mp \frac{H_z\sigma_r'}{\omega})^2 + (\frac{\sigma_r}{\omega} + \frac{H_z\sigma_i'}{\omega})^2}\right]$$

Using these values of refractive index and the equation

$$\theta = \frac{t\pi}{2\lambda\eta}(\eta_-^2 - \eta_+^2)$$

we can now evaluate θ in terms of the conductivity. In the low field case in which terms in H_z^2 are neglected and assuming again that the absorption is small we obtain (T1) the expression

$$\theta = \frac{tc\mu H_z\sigma_r'}{2\eta} \qquad (2.16)$$

This low field approximation has appeared before when it was assumed that for the cyclotron frequency (which is proportional to H_z) was small compared to the frequency of the radiation. As long as this is the case then the equation (2.16) is valid and θ has now been expressed in terms of the conductivity of the specimen.

2.3 BOLTZMANN THEORY

i Introduction

The main purpose of this section of the theory is to relate the conductivity σ_r' that was obtained in the previous section to the band parameters. The method used is to first obtain an expression for the Fermi distribution function in the presence of external

forces. This term is then substituted into the expression for the current density and by comparison with a previous equation the value for σ_r' is extracted. At this point σ_r' is expressed in terms of the band parameters. Utilizing equation (2.16), we then may evaluate the rotation in terms of the band parameters.

ii Evaluation of σ_r' in Terms of the Band Parameters

(a) The Boltzmann Equation

The Boltzmann equation considers three effects on the transport of carriers: (a) diffusions, (b) fields and (c) collisions in terms of the Fermi distribution function. In the steady state the total rate of change is zero, which is expressed as

$$\dot{f}_k = \dot{f}\Big]_{\text{diff.}} + \dot{f}_k\Big]_{\text{field}} + \dot{f}_k\Big]_{\text{coll.}} = 0 \qquad (2.17)$$

For small deviations from equilibrium the collision term may be written as

$$\left[\frac{df_k}{dt}\right]_{\text{coll.}} = -\left[\frac{f - f_o}{\tau}\right] \qquad (2.18)$$

In other words, we assume that the rate of relaxation is proportional to the deviation of the function from equilibrium. Here τ is the relaxation time and f_o is the form of the function f corresponding to thermal equilibrium. For small deviations from equilibrium it would appear that this equation is justified but for non-isotropic crystals τ is not necessarily a scalar quantity. The time of

relaxation is clearly of the same order of magnitude as the time between collisions but the numerical factor connecting them can only be determined when an exact definition of the latter time has been adopted.

For an isothemal semiconductor $\left[\frac{df}{dt}\right]_{diff.} = 0$ so that for the steady state

$$\left[\frac{\partial f(k)}{\partial k}\frac{\partial k}{\partial t}\right]_{fields} - \left[\frac{\partial f(k)}{\partial t}\right]_{coll.} = 0 \qquad (2.19)$$

Since the Lorentz force is $\vec{F} = e(\vec{E} + \vec{v} \times \vec{B})$ we obtain

$$-\frac{e}{h}(\vec{E} + \vec{v} \times \vec{B}) \cdot \nabla_k f_k + \frac{f_k - f_o}{\tau} = 0 \qquad (2.20)$$

which is the Boltzmann equation for an isothermal semiconductor. We now introduce a new function Φ_k defined by

$$f_k = f_o - \Phi \frac{\partial f_o}{\partial E}$$

This function is just a measure of the deviation from equilibrium in the electron distribution, weighted with a factor which depends on the form of that distribution. In fact it is the extra energy that the particles have because of the transport process. If we substitute this equation into the Boltzmann equation for an isothermal semiconductor then we obtain an equation in Φ

$$\frac{\Phi}{\tau} + \frac{e}{\hbar}\vec{E} \cdot \nabla_k E + \frac{e}{\hbar^2}\vec{B} \cdot \nabla_k E \times \nabla_k \Phi = 0 \qquad (2.21)$$

which has been solved for Φ by Jones and Zener (34 J1). The solution obtained is

$$\Phi = -\frac{e}{\hbar}\left\{ \vec{\tau E} \cdot \vec{\nabla}_k E - \frac{e}{\hbar^2} \vec{\tau B} \cdot \vec{\nabla}_k E \times \vec{\nabla}_k (\vec{\tau E} \cdot \vec{\nabla}_k E) \ldots\ldots + \right\} \qquad (2.22)$$

where higher order terms are neglected.

(b) Current Density

The current density $\vec{J}$ is equal to the electronic charge times the velocity summed over all the carriers in K space

$$\vec{J} = \int_0^\infty e\,(f_k)\,\vec{v}\,\frac{d^3k}{4\pi^3}$$

where $d^3k = dk_x\,dk_y\,dk_z$ is the volume element. The number of electronic states per unit volume associated with an element $dk_x\,dk_y\,dk_z$ of space is (including spin) $\frac{1}{4\pi^3} dk_x\,dk_y\,dk_z$. The average number of occupied states is $\frac{f_k}{4}\,dk_x\,dk_y\,dk_z$. Now if we substitute $f = f_o - \Phi \frac{\partial f_o}{\partial E}$ into the equation we obtain

$$\vec{J} = -\frac{e}{4\pi^3}\int_0^\infty \frac{\vec{\nabla}_k E}{\hbar}\left(f_o - \Phi \frac{\partial f_o}{\partial E}\right) d^3k \qquad (2.24)$$

The term f_o does not contribute anything to the current since it is spherically symmetric with respect to k. By using $f_o - \Phi \frac{\partial f_o}{\partial E}$

we emphasize the fact that the current is essentially determined by the deviation $f_o - \Phi \frac{\partial f_o}{\partial E}$ from the Fermi distribution. Substituting for Φ we obtain for the current density $\vec{J}$

$$\vec{J} = -\frac{e}{4\pi^3\hbar}\int_o^\infty \frac{\partial f_o}{\partial E}\vec{\nabla}_k E\left(-\frac{e\tau}{\hbar}\vec{E}\cdot\vec{\nabla}_k E\right)d^3k$$

$$+\frac{e}{4\pi^3\hbar}\int_o^\infty \frac{\partial f_o}{\partial E}\vec{\nabla}_k E\left(\frac{e^3}{\hbar^3}\tau\,\vec{B}\cdot\vec{\nabla}_k E\times\vec{\nabla}_k(\tau\vec{E}\cdot\vec{\nabla}_k E)\right)d^3k$$

$$=\frac{e^2}{4\pi\hbar^2}\int_o^\infty \tau\frac{\partial f_o}{\partial E}\vec{\nabla}_k E\cdot\vec{E}\cdot\vec{\nabla}_k E\,d^3k$$

$$-\frac{e^3}{4\pi^3\hbar^4}\int_o^\infty \tau^2\frac{\partial f_o}{\partial E}\vec{\nabla}_k E\cdot\left(\vec{B}\cdot\vec{\nabla}_k E\times\vec{\nabla}_k(\vec{E}\cdot\vec{\nabla}_k E)\right)d^3k \qquad (2.25)$$

If we consider an alternating electric field we must modify our equations. For the d.c. case the displacement of the Fermi sphere by an applied field $\vec{E}$ is

$$\vec{\delta k} = \frac{e\vec{E}\tau}{\hbar} = \frac{e\vec{E}}{\hbar}\left(\frac{1}{\tau}\right)^{-1}$$

In the alternating case $\vec{E}$ is of the form $E = Eoe^{-i\omega t}$ and so the displacement of the Fermi sphere becomes

$$\vec{\delta k} = \frac{e\vec{E}}{\hbar}\left(\frac{1}{\tau} + i\omega\right)^{-1}$$

As a result in order to obtain expressions for the alternating field case we replace τ by $(\tau^{-1} + i\omega)^{-1}$ and τ^2 by $(\tau^{-1} + i\omega)^{-2}$. At high frequencies $\omega\tau >> 1$ and these terms reduce to

$$\left(\frac{1}{\omega^2\tau} - \frac{i}{\omega}\right) \quad \text{and} \quad -\left(\frac{1}{\omega^2} + \frac{2i}{\omega^3\tau}\right)$$

Substituting these terms into the equation for the current density we obtain

$$\vec{J} = \frac{e^2}{4\pi\hbar^2\omega^2}\int_0^\infty \frac{1}{\tau}\frac{\partial f_o}{\partial E}\,\vec{\nabla}_k E \cdot \vec{E} \cdot \vec{\nabla}_k E \; d^3k$$

$$- \frac{e^2 i}{4\pi\hbar^2\omega}\int_0^\infty \frac{\partial f_o}{\partial E}\,\vec{\nabla}_k E \cdot \vec{E} \cdot \vec{\nabla}_k E \; d^3k$$

$$+ \frac{e^3}{4\pi^3\hbar^4\omega^2}\int_0^\infty \frac{\partial f_o}{\partial E}\,\vec{\nabla}_k E \cdot \vec{B} \cdot \vec{\nabla}_k E \times \vec{\nabla}_k (\vec{E} \cdot \vec{\nabla}_k E) \; d^3k$$

$$+ 2\,\frac{e^3 i}{4\pi^3\hbar^4\omega^3}\int_0^\infty \frac{1}{\tau}\frac{\partial f_o}{\partial E}\,\vec{\nabla}_k E \cdot \vec{B} \cdot \vec{\nabla}_k E \times \vec{\nabla}_k (\vec{E} \cdot \vec{\nabla}_k E) \; d^3k \qquad (2.26)$$

If we now make a direct comparison of this equation with that previously derived in the foregoing section,

$J_i = (\sigma_r + i\sigma_i)\,\delta_{ij}E_j + (\sigma_r' + i\sigma_i')\,\epsilon_{ijk}\,E_j\,H_k$, we see that

$$\sigma_r' \varepsilon_{ijk} E_j H_k = \frac{e^3}{4\pi^3\hbar^4\omega^2}\int_o^\infty \frac{\partial f_o}{\partial E} \vec{\nabla}_k E \cdot \vec{B} \cdot \vec{\nabla}_k E \times \vec{\nabla}_k (\vec{E} \cdot \vec{\nabla}_k E)\, d^3k \tag{2.27}$$

We have now obtained the value for σ_r' in terms of the band parameters and are now ready to substitute this value into the expression for the rotation.

iii Relationship between θ and the Band Parameters

From the section on conductivity theory, the value that was obtained for the rotation was $\theta = \frac{t\, c\, \mu\, H_z}{2n}\, \sigma_r'$. If we now substitute the value for σ_r' we obtain

$$\theta = \frac{45\, e^3 t\, B\lambda^2}{8\pi^6\hbar^4 c^3 \varepsilon_o n}\int_o^\infty \frac{\partial f_o}{\partial E} \frac{\partial E}{\partial k_x} \left\{ \frac{\partial E}{\partial k_y} \cdot \frac{\partial^2 E}{\partial k_x \partial k_y} - \frac{\partial E}{\partial k_x} \cdot \frac{\partial^2 E}{\partial k^2_y} \right\} d^3k \tag{2.28}$$

A factor of $\frac{180}{\pi}$ has been introduced to convert from radians to degrees. We let

$$I_1 = \int_o^\infty \frac{\partial f_o}{\partial E} \frac{\partial E}{\partial k_x} \left\{ \frac{\partial E}{\partial k_y} \frac{\partial^2 E}{\partial k_x \partial k_y} - \frac{\partial E}{\partial k_x} \frac{\partial^2 E}{\partial k^2_y} \right\} d^3k \tag{2.29}$$

$$I_2 = \int_o^\infty f_o\, d^3k \tag{2.30}$$

where $N = \frac{2}{(2\pi)^3}\int_0^\infty f_o \, d^3k$ is the relation for the carrier concentration. Then we see that

$$\theta = \frac{45\, e^3 t\, B\, N\, \lambda^2}{2\, \pi^3\, \hbar^4\, c^3\, \epsilon_o\, n} \frac{I_1}{I_2}$$

If we compare this equation with equation(2.7)

$$\theta = \frac{N\, e^3 t\, B\, \lambda^2}{8\, \pi^2\, c^3\, \epsilon_o\, \hbar\, m^*_{ic}{}^2}$$

we can obtain an expression for the Faraday effective mass in terms of I_1 and I_2

$$\frac{m^*_{if}}{m} = \left(4a^2 \frac{I_2}{I_1}\right)^{\frac{1}{2}} \qquad (2.31)$$

where I_1 and I_2 have previously been defined and $a = \frac{\hbar^2}{2m}$.

2.4 KANE THEORY

i Introduction

The end product of the Kane theory (56 K1, 57 K1) is to provide a model of the conduction band which we can use to determine the particular value of the rotation in terms of the bottom of the band effective mass. The previous section obtained the rotation in terms of the derivatives of the energy and the distribution

function. In this section, I shall briefly present the results of the Kane theory and then proceed to derive the value for θ based on Kane's model for the conduction band. From there I shall show how it is possible to determine the variation of the effective mass as a function of composition.

ii Results of the Kane Theory

Beginning with the Schrodinger equation and using the k·p perturbation approach, Kane obtained a solution to the resultant secular determinant at $k = 0$. The resulting equation is at absolute zero

$$(E' + E_o)\left\{ E' (E' + E_o) (E' + E_o) (E' + E_o + \Delta_o) - ak^2 P^2 \right.$$

$$\left. (E' + E_o + \frac{2}{3}\Delta_o)\right\} = 0 \qquad \text{where } a = \frac{\hbar^2}{2m} \quad \text{and } E' = E - ak^2$$

which is the energy minus the free electron energy. E_o is the fundamental gap at absolute zero, Δ_o is the valence band spin orbit splitting and P^2 is the momentum matrix element. For the solution at higher temperatures, Ehrenreich (57 E1) has shown that E_o may be replaced by E_o^* , an effective mass band gap. If P^2 is expressed in terms of the effective mass assuming

$$E - ak^2 < E_o^* + \frac{2}{3}\Delta_o$$

the equation reduces to (T1):

(2.32)

$$E = ak^2 + \frac{E_o^*}{2}\left[\left\{1 + \frac{4a}{E_o^*}\left(\frac{m}{m_{oo}^*} - 1\right)k^2\right\}^{\frac{1}{2}} - 1\right]$$

which will be the model used for the conduction band.

iii Evaluation of θ

From equation (2.28) we know that

$$\theta = \frac{45\ e^3 t\ B\lambda^2}{8\pi^6\hbar^4 c^3 \varepsilon_o n}\int_o^\infty \frac{\partial f_o}{\partial E}\ \frac{\partial E}{\partial k_x}\left[\frac{\partial E}{\partial k_y}\ \frac{\partial^2 E}{\partial k_x \partial k_y} - \frac{\partial E}{\partial k_x}\ \frac{\partial^2 E}{\partial k^2_y}\right] d^3k$$

where $f_o = (\exp\ (E - E_f) / KT + 1)^{-1}$ and

$$E = ak^2 + \frac{E_o^*}{2}\left[\left\{1 + \frac{4a}{E_o^*}\left(\frac{m}{m_{oo}^*} - 1\right)k^2\right\}^{\frac{1}{2}} - 1\right]$$

If we now proceed to do a term by term evaluation of each derivative we obtain for the rotation

$$\theta = \frac{60\ e^3\ a^3\ t\ B\lambda^2}{\pi^5\hbar^4\ c^3\ \varepsilon_o n\ KT}\ I_1' \qquad (2.33)$$

where

$$I_1' = \int_o^\infty \frac{k^4\left[1 + \left(\frac{m}{m_{oo}^*} - 1\right)\left\{1 + \frac{4a}{E_o^*}\left(\frac{m}{m_{oo}^*} - 1\right)k^2\right\}^{-\frac{1}{2}}\right]^3 dk}{2 + \exp\left\{\frac{E - E_{fo}}{KT}\right\} + \exp\left\{\frac{E_{fo} - E}{KT}\right\}}. \qquad (2.34)$$

and since the carrier concentration N is $N = \frac{1}{\pi^2}\int f_o\, k^2\, dk$

then $N = \frac{I_2'}{\pi^2}$ where $I_2' = \int \frac{k^2 dk}{1 + \exp\left\{\frac{E - E_{fo}}{KT}\right\}}$ (2.35)

Again if we compare this equation with equation (2.7)

$$\theta = \frac{N e^3 t B\lambda^2}{8 \pi^2 c^3 \epsilon_o \eta m^{*2}_{fc}}$$

we find that

$$\frac{m^*_{of}}{m} = \left[\frac{3\ KT}{2a}\ \frac{I_2'}{I_1'}\right]^{\frac{1}{2}} \qquad (2.35)$$

iv Method of Analysis

The experimental values of I_1' and I_2' may now be evaluated in terms of the conduction band parameters. For each sample we know the percent composition from the x-ray data. Knowing this we can obtain the value of E* which we set equal to

$\frac{E_{oo} + E_o}{2}$ where E_{oo} is the fundamental gap at absolute zero and E_o is the fundamental gap at room temperature. This is done because it was found by Smith et. al. (62S1) that this was the best form to fit the Faraday rotation data for InSb. In any case it is found that the values determined for m^*_{oo} are

not very sensitive to small variations in E_o^* .

The integrals contain two other unknowns m_{oo}^* , the effective mass at the bottom of the conduction band and Ef_o , the Fermi energy. From experimental results we have values for both I_1' and I_2' . For any chosen value of m_{oo}^* we can vary the Fermi energy until the experimental value I_1' is obtained. For the same effective mass m_{oo}^* , we can again vary the Fermi energy until the value for I_2' is obtained. In general the two values of Ef will not be the same. However, if we plot on a graph of m_{oo}^* vs Ef_o the solutions (m_{oo}^*, Ef_o) for each of I_1' and I_2' , then we obtain two curves which intersect at a common solution (m_{oo}^*, Ef_o). This value is taken as the bottom of the band effective mass of the sample.

A further refinement must be added since the calculations involve the refractive index which for heavy doping is a function of the wavelength. Because of this the refractive index must be modified if the carrier concentration is large.

III METHOD

3.1 SAMPLE PREPARATION

(a) Ingots Growth

The samples studied in this thesis were cut from the GaSb rich end of $GaAs_xSb_{1-x}$ ingots grown in this department by Dr. Stanley Rosenbaum. Three ingots were used as a source of samples: TZF-4, TZF-5 and TZF-6 and all had been doped with Te, a donor impurity. These ingots had been grown using the horizontal Bridgman technique with a pull rate of less than 1 cm. per day. This ensured that homogeneous results would occur. Unfortunately the GaAs rich end of the ingots were p-type and so could not be used. The mechanics of the growth of these ingots has previously been described in the introduction and for the interested reader further information may be found in S. Rosenbaum's doctoral thesis (R1).

(b) Sample Preparation

Once an ingot had been selected, samples were cut from it using a spark cutter. The spark cutter consists of a travelling wire charged to a preset voltage. The wire and work piece are immersed in a kerosene dielectric and a servomotor drives

the wire assembly down to the work piece which is grounded. Eventually the wire comes close enough for the voltage to breakdown the dielectric between the work piece and the wire. The resulting spark is sufficiently hot enough to melt micro-pits in the sample. A feed-back system adjusts the rate of downward travel of the wire electrode. The advantage of this cutting method is that it introduces very little damage to the sample and produces a minimum loss of material.

After the samples had been cut from the ingot they were then mounted on a lapping block and lapped down to a few hundred microns using a 5 micron grit. The faces were lapped parallel and then were polished to a mirror finish using a 1 micron powder and a rotating polishing pad. The resulting samples were square, 6 mm. on each side and varying in thickness from 60 microns to 200 microns, depending on how heavily doped they were. The more highly doped samples were more absorbing so the thickness was made inversly proportional to the carrier concentration. Thicknesses were measured using both a micrometer marked off into 2 micron divisions and a vernier probe. The final value was taken as the average of all readings.

Finally the samples were given a degrease in solvents and then blown dry. At this point they were ready for magneto-optical experiments.

3.2 MAGNETO-OPTICAL EXPERIMENTS

The equipment used to measure the rotation as a function of the wavelength is shown in Fig. 3.1. The equipment consisted of three basic parts which will be dealt with individually.

(a) The Optical System

The heart of the optical system was a Perkin-Elmer monochrometer which used a Nernst filament source. This source gave a high intensity of radiation in the wavelength range that was used (2 to 13 microns). The radiation was focused onto a NaCl prism which was attached to a revolving table within the monochrometer. By rotating this prism, different wavelengths could be made to fall on the exit slit. The prism was interchangeable and for wavelengths longer than 15 microns a KBr prism could be used. Within the monochrometer, a blade rotating at 12.5 c.p.s. chopped the radiation.

The general procedure when using the monochrometer was to adjust the internal mirrors to maximize the radiation at the exit slit. After this, the setting on the drum which turned the prism had to be calibrated in terms of the wavelength. To do this a scan was done using different filters and the read-out analysed. By studying the known absorption of air, polystyrene etc. a graph of wavelength versus drum setting could be plotted

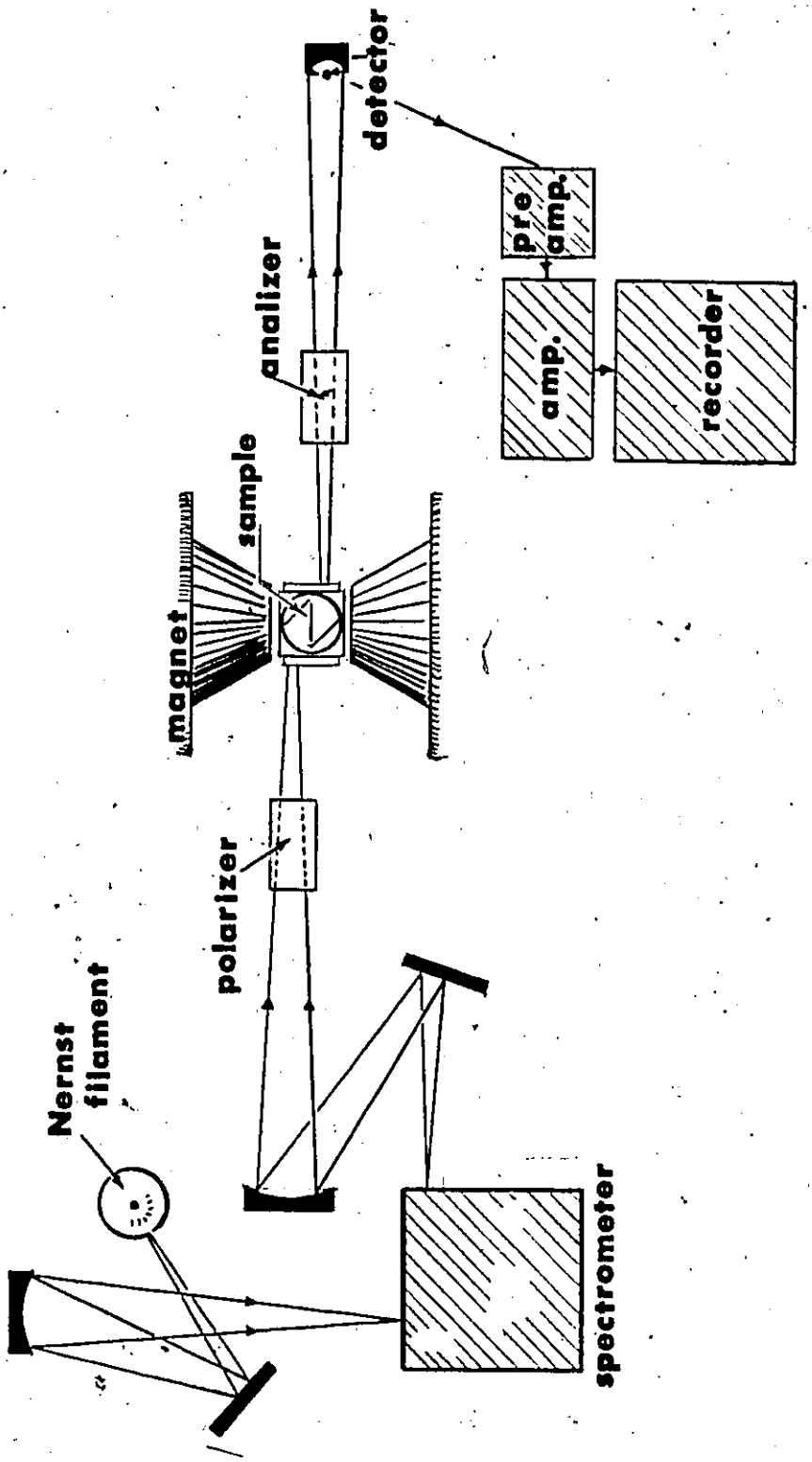

Fig. 3.1. The Faraday rotation equipment.

(see Fig. 3.2). Before every measurement the calibration was checked by locating a large, easily recognized absorption band and making sure that the drum reading corresponded to this wavelength.

After leaving the exit slit the radiation was focussed through a Beckman silver chloride pile-of-plates polarizer onto the sample. For liquid nitrogen temperature measurements the sample was contained in an evacuated cryostat at the end of a copper cold finger. Small mirrors placed at 45° to the sample, permitted the radiation to pass through the sample in the same direction as the magnetic field. The chamber had KBr windows to minimize absorption in the infrared.

After leaving the sample the radiation passed through another pile-of-plates analyzer that was rotated slowly by a motor. The radiation was then focused onto an infrared detector and the signal was measured.

(b) Electrical System

The chopped signal was passed from the detector to a transformer and from there to a pre-amplifier. The pre-amplifier was connected to a lock-in amplifier which in turn was connected to an x-y recorder. The x-y recorder measured voltage along one axis and time along the other. Several minutes were needed to complete a revolution of the analyzer and the resulting curve

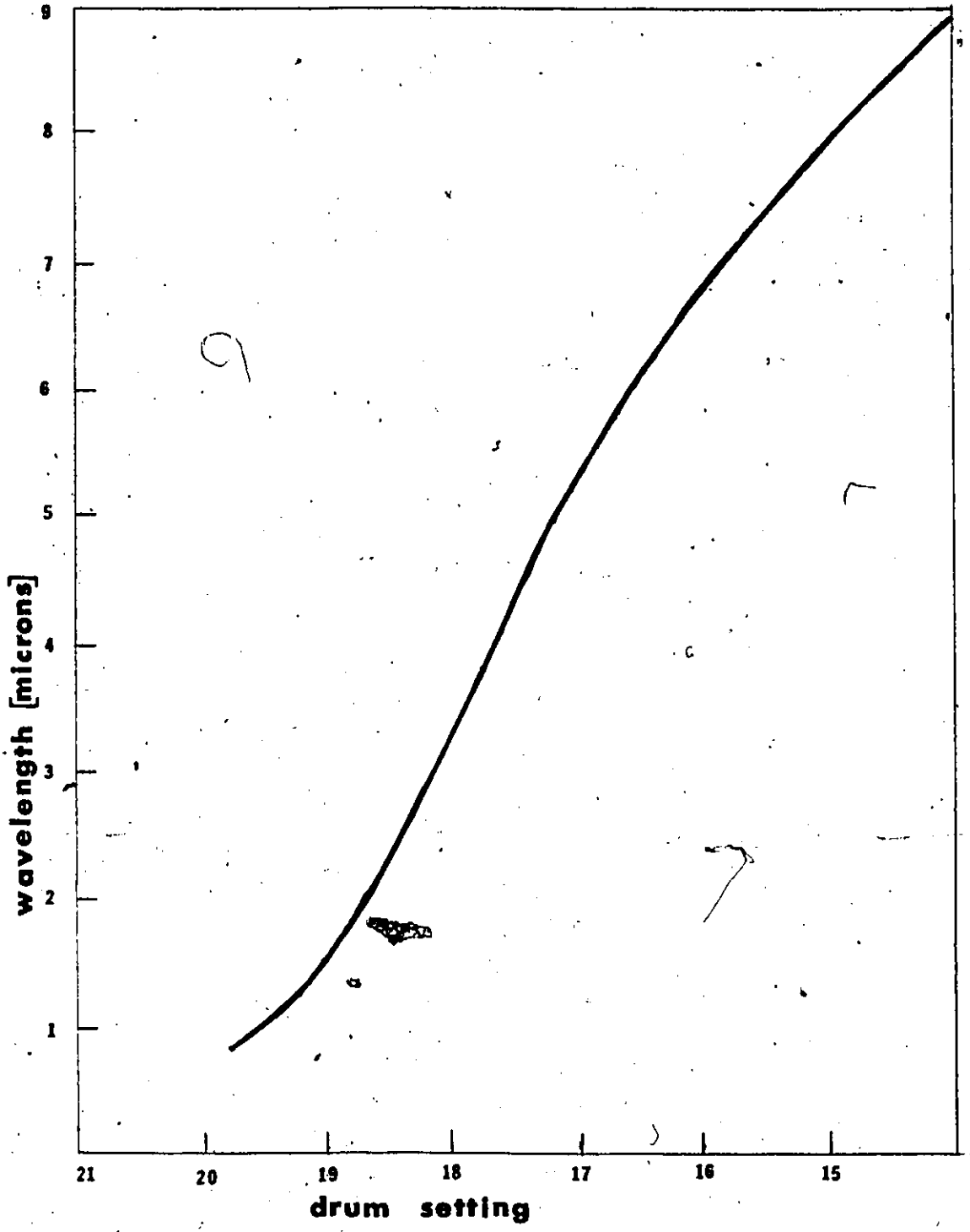

Fig. 3.2 Calibration curve for the NaCl prism from 1 to 9 microns.

was sinusoidal, see Fig. 3.3. After one revolution, the magnetic field was reversed and the x-y recorder was again zeroed and the analyzer was permitted to rotate once more. This time the curve was shifted from the original position by a value of 2θ where θ is the Faraday rotation. The phase shift was determined from an average of several points on the curve.

(c) The Magnetic System

The magnetic system consisted of a Harvey-Wells "Magnion" magnet capable of delivering a maximum field of 32 kilogauss uniformly over a spacing of 4 cm. The field was stabilized by a feedback system using a Rawson Gaussmeter probe. Before measurements were taken the magnetic field was calibrated.

3.3 VAN DER PAUW MEASUREMENTS

(a) Sample Preparation

Contacts were made at the four corners of each sample. Most samples gave good results using a small ball of conductive epoxy to provide adherence for the gold wire to the corner of the sample. A series of measurements were done using this type of contact. Occasionally non-ohmic contacts would result so a second set of measurements were done using Au-Sn wire spark welded to the corners, after having removed the epoxy. These gave ohmic results.

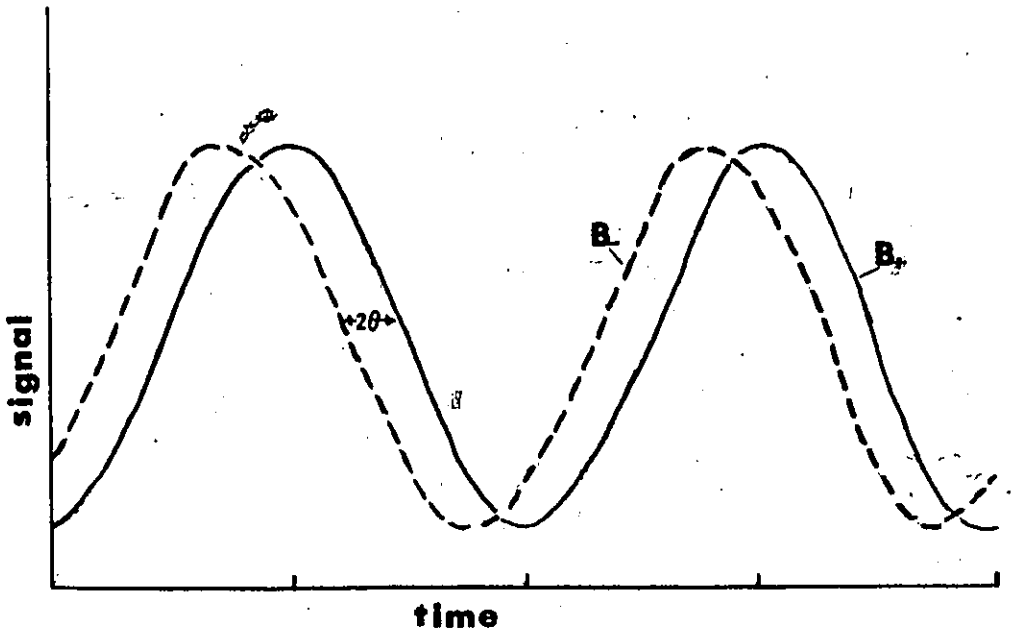

Fig. 3.3 Sinusoidal traces resulting from the rotation of the analyzer with a fixed polarizer.

(b) Sample Holder and Current Source

The sample holder for room temperature measurements consisted of a non-magnetic insulating base plate on which the sample was placed flat. The gold wires were soldered with indium to pads which in turn were connected to the current source leads, see Fig. 3.4. For liquid nitrogen temperatures a cryostat and cold finger set-up was used.

A constant current source was used in the measurements and this current was reversed through the sample at 10 c.p.s. by a chopping switch. The voltage across the sample, which was measured using a chart recorder, was synchronously reversed at the same rate. The use of a chart recorder permitted a reading to be taken when equilibrium was established and also made any zero shifts apparent. The current was measured by taking the voltage across a standard resistance. A potentiometer placed in parallel with the chart recorder permitted the voltage to be zeroed prior to application of the magnetic field. After a measurement was done, the field was reversed and the Hall voltage was measured in the reverse direction. The magnet was the same as that used for the magneto-optical measurements and Hall coefficients could be measured with fields as high as 32 kilogauss. Fig. 3.5 shows the experimental set-up for Van der Pauw measurements.

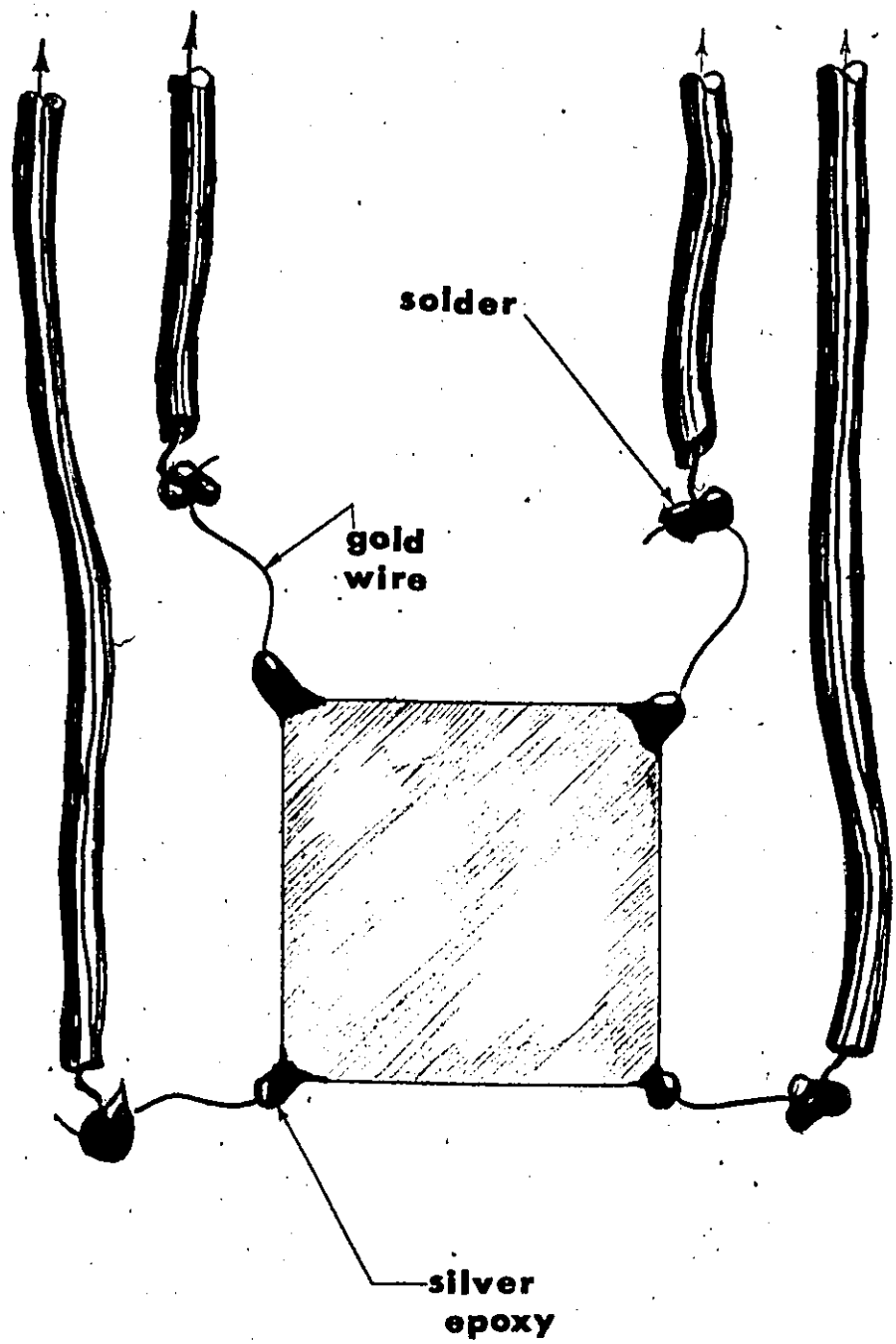

Fig. 3.4 Sample and connections to the current source leads.

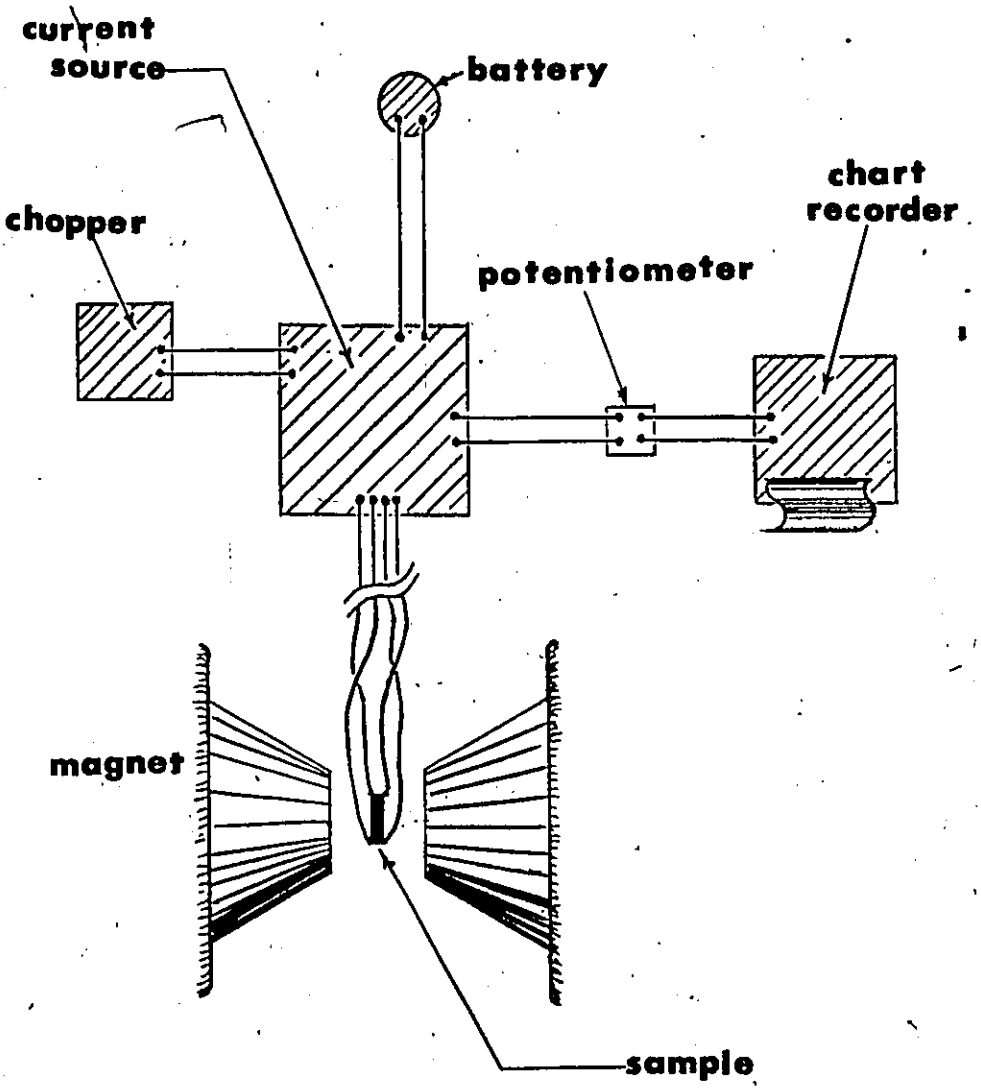

Fig. 3.5 Van der Pauw equipment.

IV RESULTS AND DISCUSSIONS

Results have been obtained for thirteen samples $GaAs_xSb_{1-x}$ varying in composition from $x = .13$ to $x = .31$, removed from ingots TZF-4, TZF-5 and TZF-6.

Three sets of measurements were made on each sample

(a) Faraday Rotation

(b) Van der Pauw Measurements

(c) X-ray Analysis.

4.1 Faraday Rotation

Practically all the Faraday rotation data had a linear variation of θ vs λ^2 as would be expected. A calculation of the reflection coefficient and the approximate absorption for the carrier concentrations used here, indicate that multiple reflection would contribute only a very small value to the total rotation. Hence it was assumed that internal reflections could be ignored. The results are shown in the following graphs and the values of the slopes are given in table 4.1.

The results for Faraday rotation at liquid nitrogen temperatures are not shown since they could not be used due to the uncertainty of values for the carrier concentration at liquid nitrogen temperature. However in all cases the slope of θ vs λ^2 increased

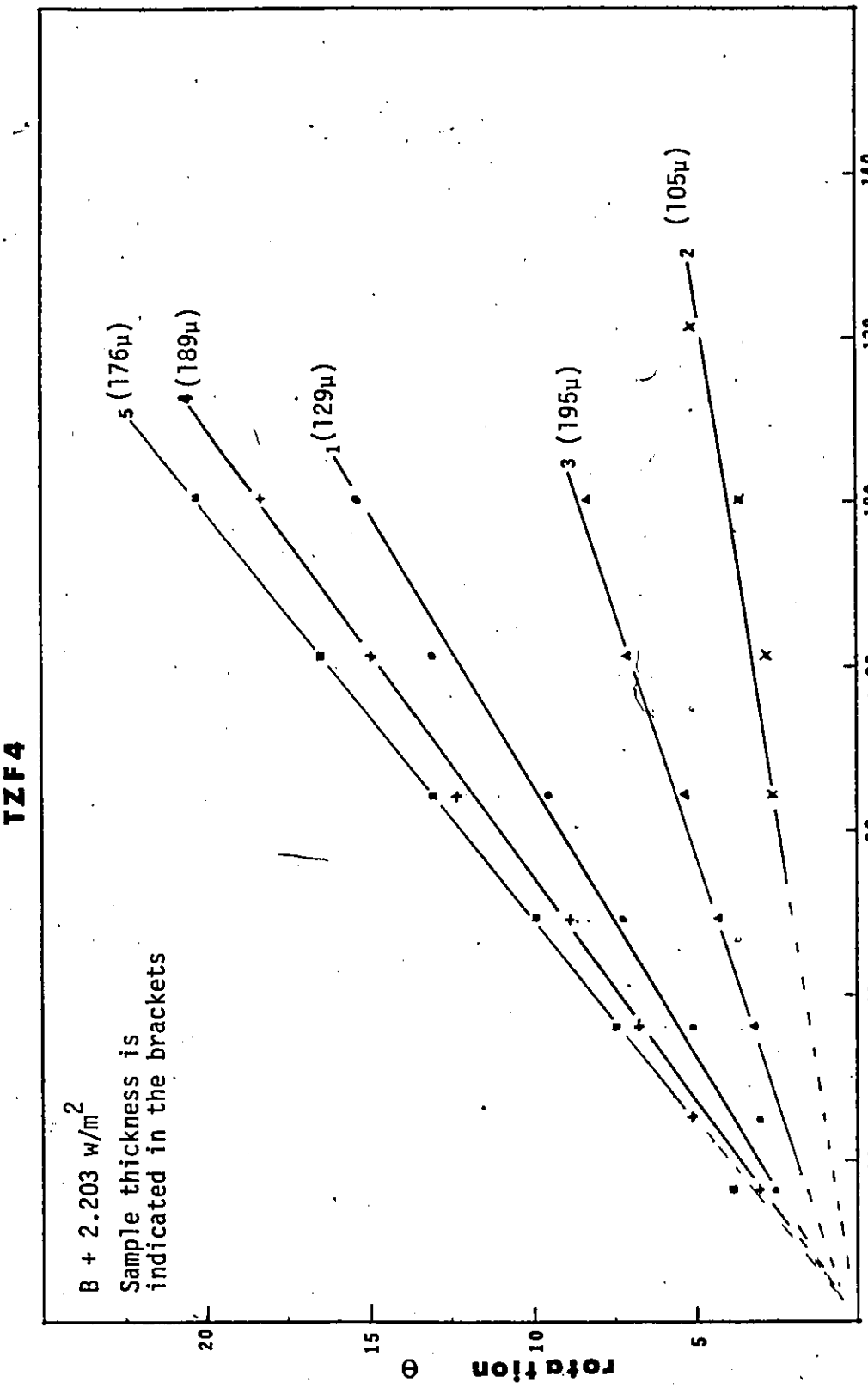

Fig. 4.1 θ vs. λ^2 for the samples from ingot TZF-4.

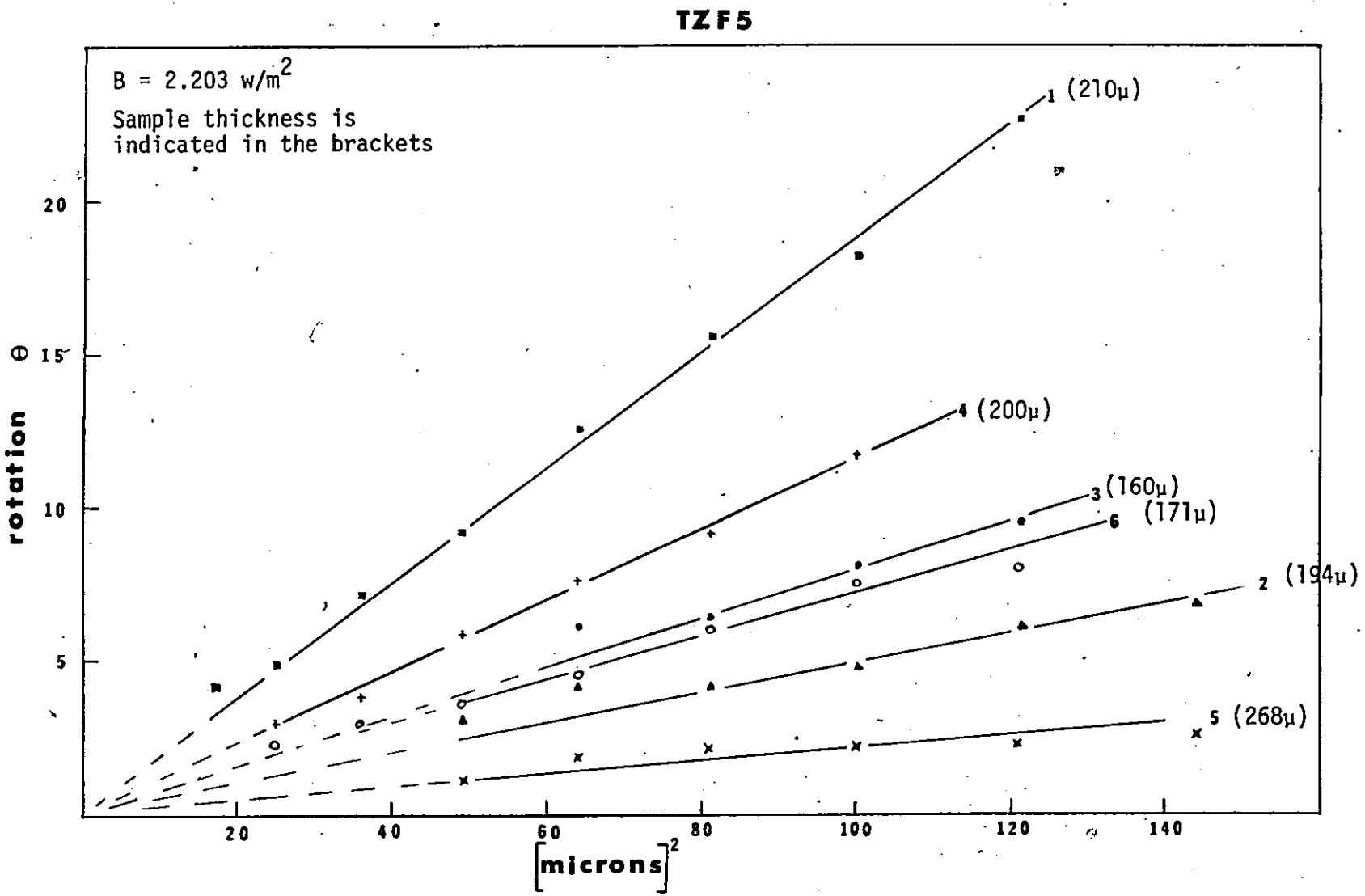

Fig. 4.2 θ vs. λ^2 for samples from ingot TZF-5

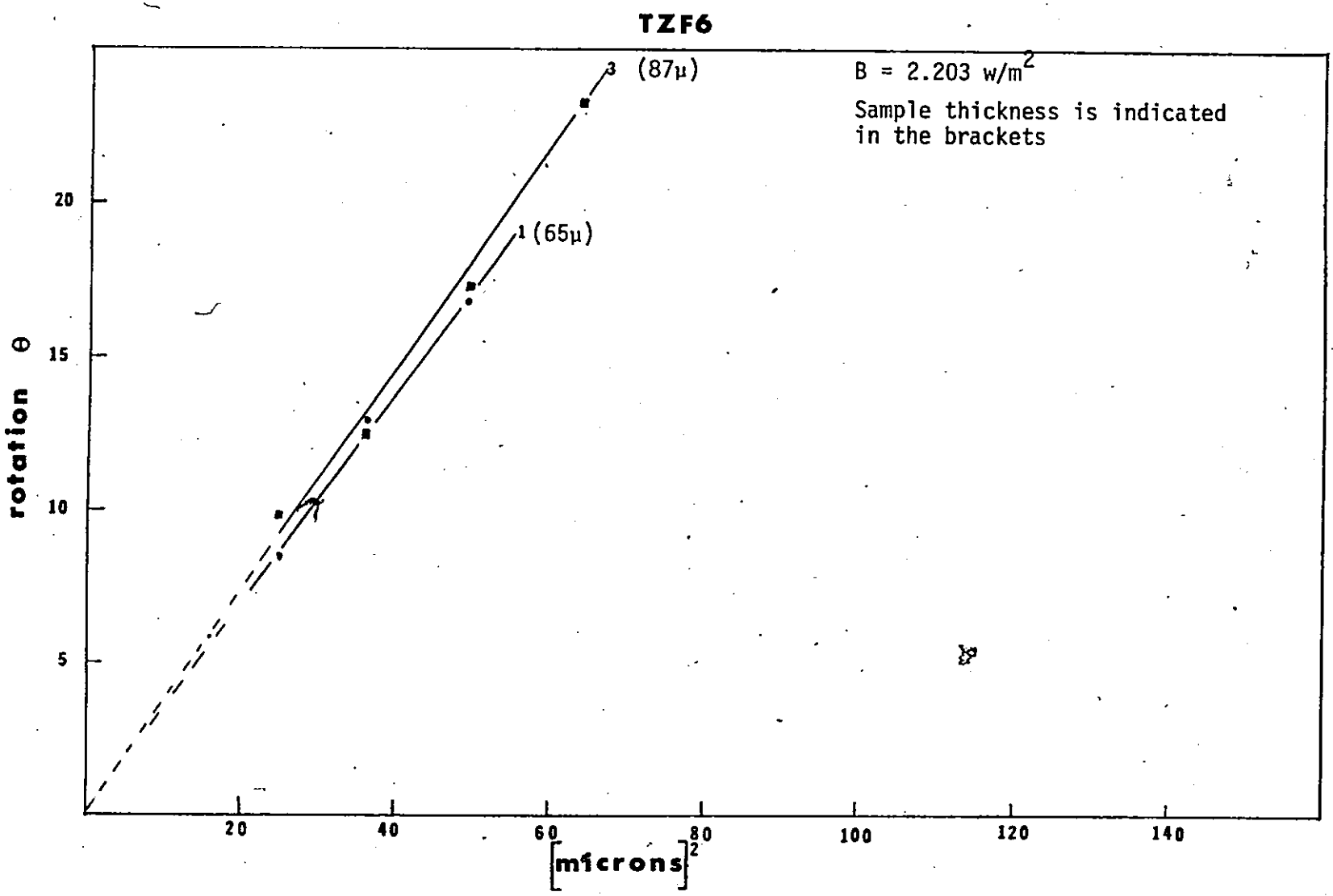

Fig. 4.3 θ vs. λ^2 for samples from ingot TZF-6.

TABLE 4-1

SAMPLE	SLOPE (θ/λ^2) 10^{12} degrees/m^2 ROOM TEMP.	LIQUID N_2 TEMP.	COMPOSITION (X)
TZF4-1	.163		.28
2	.044		.13
3	.074	.102	.14
4	.177	.216	.24
5	.198		.16
TZF5-1	.182		.27
2	.044	.066	.24
3	.078	.090	.22
4	.118	.127	.23
5	.019	.023	.23
6	.074	.078	.19
TZF6-1	.348	.425	.31
3	.353		.15

with decreasing temperature. Since $\frac{\theta}{\lambda^2} \propto$ (constant) $\frac{N}{m^*_{oo}{}^2}$, this indicates that the ratio $\frac{N}{m^*_{oo}{}^2}$ is increasing. An explanation of this effect is given later on in this section.

4.2 VAN DER PAUW RESULTS

Room temperature measurements were made on all samples and some attempt was made to measure the carrier concentration at liquid nitrogen temperature. The latter results were poor, however due to a low signal to noise ratio.

The equation (58 P1) used to obtain the Hall coefficient is given by

$$R_h = \frac{\Delta R t}{B} \times 10^{-5} \text{ cm}^3/\text{c}$$

where t is the sample thickness, B is the magnetic field in kilogauss and ΔR is the resistance obtained by passing a current through one pair of diagonally opposed contacts and measuring the potential across the other pair. All measurements were taken as a function of magnetic field strength so that a saturation value for the Hall coefficient could be found. The results are summarized in table 4.2.

TABLE 4-2

SAMPLE	CARRIER CONCENTRATION (10^{17} cm^{-3})	COMPOSITION (X)
TZF4-1	4.8	.28
2	1.1	.13
3	1.5	.14
4	3.5	.24
5	3.7	.16
TZF5-1	2.5	.27
2	.8	.24
3	1.5	.22
4	2.1	.23
5	.2	.23
6	1.2	.19
TZF6-1	27.	.31
3	17.	.15

4.3 X-RAY RESULTS

A representative section of each sample was powdered and x-rayed by G. Goodchild. The x-rays indicated that the samples were homogeneous. The composition was determined from a graph of lattice parameter vs composition for $GaAs_xSb_{1-x}$ taken from the work of Gratton and Woolley (73 G1). The results are summarized in table 4.3 along with the values for the refractive index.

4.4 ANALYSIS

Equation 2.33 expresses I_1' in terms of the Faraday rotation data i.e. $\frac{\theta}{\lambda^2} =$ (constant) $\frac{Bt}{\eta}$ I_1' where the constant has a value of 2.093×10^{25}, θ/λ^2 is obtained from the Faraday rotation data and $\frac{Bt}{\eta}$ is known. As a result we may readily obtain an experimental value of I_1'. Similarly an experimental value of I_2' may also be found since $I_2 = \pi^2 N$. However both I_1' and I_2' may be also derived from the integrals in equations 2.34 and 2.35. To evaluate these integrals we require values for m_{oo}^*, and E_f and E_o^*. The procedure used was to substitute a value of E_o^* and m_{oo}^* and find the value of I_1' and I_2' over a range of E_f. Then m_{oo}^* was changed and a new set of I_1' and I_2' found. For each m_{oo}^* value there exists values of E_f for which the I_1' (theoretical)

TABLE 4.3

SAMPLE	COMPOSITION(x)	REFRACTIVE INDEX
TZF4-1	.28	3.68
2	.13	3.76
3	.14	3.76
4	.24	3.71
5	.16	3.75
TZF5-1	.27	3.69
2	.24	3.71
3	.22	3.72
4	.23	3.71
5	.23	3.71
6	.19	3.73
TZF6-1	.31	3.67
3	.15	3.75

and I_2' (theoretical) equal the I_1' (experimental) and I_2' (experimental). If this process is repeated over several effective mass values, then curves of solutions for I_1' and I_2' are generated and at the point at which they cross a common solution of m_{oo}^* and E_f for both I_1' and I_2' is obtained. The effective mass obtained by this process is that value that gives the correct experimental results for both the Faraday rotation data and the carrier concentration data and so may be taken as the bottom of the band effective mass for the sample (see Fig. 4.4). The program used to evaluate these integrals is listed in the index.

The analysis used for these samples was a single band analysis. This was justified since doping concentrations were relatively small and the contribution of the <111> band electrons to the rotation would be minimal, because of their much larger effective masses. It should be kept in mind that the rotation is inversely proportional to the square of the effective mass. However it is possible that one sample, TZF6-3 could have a small contrition to the rotation due to the <111> band. This would be a result of its large carrier concentration combined with its high Sb concentration. A two band analysis would probably give a slightly smaller effective mass value for this sample but it would not be more than 2%.

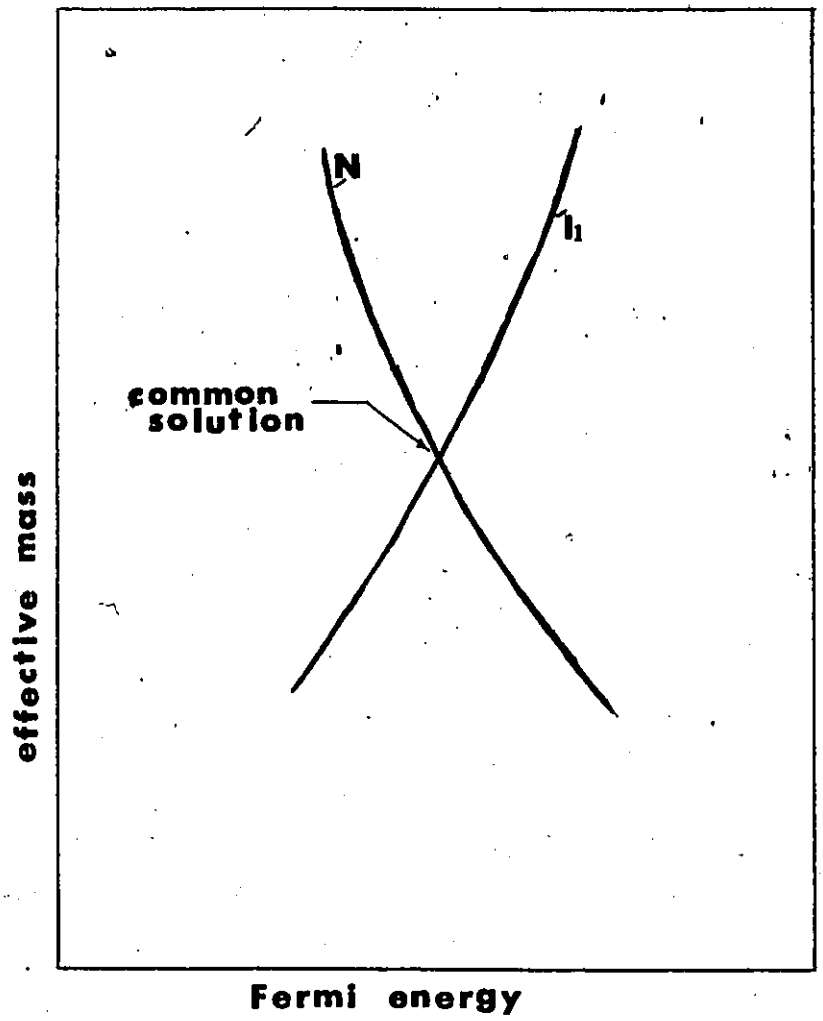

Fig. 4.4 Method of obtaining the common solution.

The solution of equations 2.33 and 2.35 for sets of values of (m^*_{oo}, E_F) require that we know the value for the refractive index and E^*_o. The refractive index for the alloy is assumed to vary linearly from GaSb to GaAs. Work done on the $GaAs_xP_{1-x}$ system (67 C1) provides some justification for this. The actual values for the refractive index of the compounds were taken from the average of published values. Although the refractive index is a function of the wavelength, it was found that for the doping level present in these samples, there was no difference between the results when η was kept constant and when η varied with wavelength.

4.5 RESULTS

The values of the effective mass for each sample are shown in Table 4.4 and also in graph 4.5 plotted as a function of composition. The first result that is apparent is the large amount of scatter present in the graph. This scatter had its origins in either the Faraday rotations or the Van der Pauw measurements. It was felt, however, that the Faraday rotation measurements were more accurate since there was very little scatter in the curves of θ vs λ^2. There was a greater possibiliy of error originating in the carrier concentration measurements. This error could have been due to the non ideal situation, in which there are rather large contact pads on a relatively small sample, resulting in shorting out

TABLE 4.4

SAMPLE	$I_1(10^{-10})$	E^*_o(ev)	m^*_{oo}	E_F(ev)	COMPOSITION (X)
TZF4-1	1.009	.72	.0487	.026	.28
2	.342	.72	.0409	-.015	.13
3	.308	.72	.0505	-.015	.14
4	.750	.72	.0487	.0137	.24
5	.915		.0454	.020	.16
TZF5-1	.682	.72	.0432	.008	,27
2	.182	.72	.0485	-.031	.24
3	.394	.72	.0445	-.009	.22
4	.475	.72	.0479	-.002	.23
5	.058	.72	.0429	-.064	.23
6	.351	.72	.0424	-.014	.19
TZF6-1	4.253	.73	.0503	.12	.31
3	3.295	.72	.0469	.09	.15

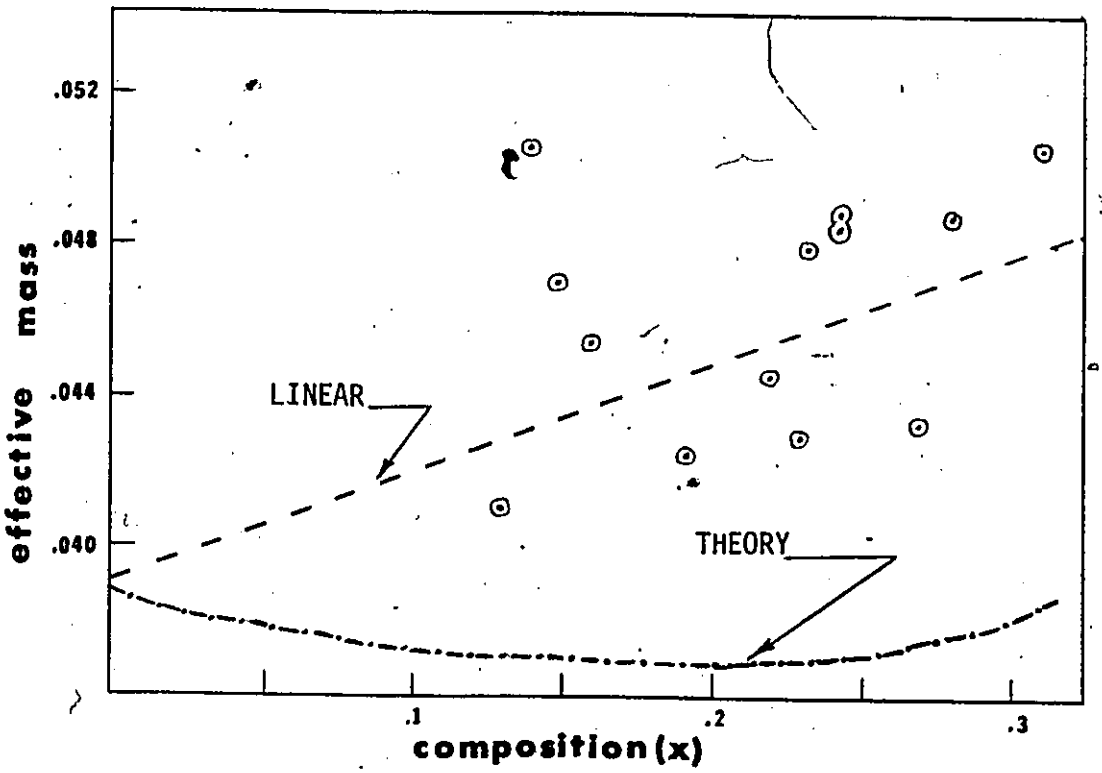

Fig. 4.5 Variation of effective mass with composition.

of part of the crystal.

The second result that is apparent is that the characteristic drop in effective mass to a minimum value, which appears in other III-V alloy systems, is not present. Barolo, Woolley and Van Vechten (73 B1) have predicted a strong dip in the variation of effective mass with composition for $GaAs_xSb_{1-x}$ and for convenience the predicted variation is included on the same graph. Although there is considerable scatter in the points the results indicate a larger effective mass than is predicted by theory. In fact the results seem to indicate that there is no dip at all and that the effective mass varies approximately linearly in this region. This larger effective mass can not be explained by a contribution from the <111> band since for the carrier concentration and the compositions used in this thesis, the contribution would be small.

In looking for a source of error in the measurements the carrier concentration was most suspect since it involved less readings than the Faraday rotation data. With this in mind, results for samples from ingot TZF-6 were compared with results of samples taken from the same ingot by S. Rosenbaum (R1). The results were found to fit very well on a curve of carrier concentration versus composition that was made from S. Rosenbaum's data. This lent more support to the correctness of the data. A further check was made using a single crystal of GaAs to determine if the overall process

gave reasonably accurate effective mass results. The result obtained for the GaAs was within the range of values expected, which gave credence to the overall process.

In order to eliminate any question of the <111> band having an effect on the measurements, calculations were made using data which represented the worst case. In this case sample TZF6-3 was the choice. This sample has a carrier concentration in the low 10^{18} cm^{-3} range and a relatively small energy separation between the Γ_1 and L_1 bands due to its high Sb concentration. To make a sample calculation I needed to know the number of carriers in the <111> band and this information was obtained from Dr. S. Rosenbaum's doctoral thesis. For this sample, whose overall carrier concentration using the Van der Pauw technique was 17×10^{17} cm^{-3}, it was found that N_o was 15×10^{17} cm^{-3}, and N_1 was 4.3×10^{17} cm^{-3}.

For a two band analysis (68 Ll)

$$\theta = \frac{45e^3tB}{2\pi^3m^2c^3\varepsilon_o}\left[\frac{N_o}{(m^*_{of}/m)^2} + \frac{N_1}{(m^*_{1f}/m)^2}\right]\frac{\lambda^2}{\eta} + \frac{AB}{\lambda^2}$$

where the λ^2 term is due to the free carrier rotation and the λ^{-2} term is due to inter-band rotation. Since N_o and N_1 are known and m^*_{of} and m^*_{1f} can be given approximate values of .045 m and .24 m respectively, we can find the percentage contributed to the rotation by the <111> electrons. In the worst case the

contribution was approximately 1%. It can be assumed then that the <111> band has little effect on the total rotation.

An explanation of the increase in rotation versus λ^2 at liquid nitrogen temperature is possible if we consider the electrons from the <111> band freezing out into the (000) band and hence providing a larger number of electrons with a much reduced effective mass. This effect would be opposed by the increasing effective mass with lowering temperature.

V CONCLUSIONS

The bottom of the band effective mass of the Γ_1 electrons in the $GaAs_xSb_{1-x}$ system has been measured for $.13 \leq x \leq .31$ and the results compared to the theoretical predictions of Berolo et. al . It was found that the results adhere closer to a linear variation of effective mass versus composition than is predicted and the reason for this is not understood. Perhaps the presence of a miscibility gap modifies the theory in some way.

In any case further work should be done to verify the results with values taken at higher As concentration. More accurate results could probably be obtained if single crystal material could be used. A great improvement in uniformity and signal to noise ratio was noticed by the author when studying single crystal GaAs as opposed to the polycrystalline alloy. The elimination of electrical barriers, which S. Rosenbaum states are present in this material, should also give better results.

APPENDIX A

The expression $\theta = \frac{\pi t}{\lambda} (\eta_- - \eta_+)$ can be derived using the relations between the refractive index and the group velocity. Consider the positive component first. The group velocity is $V+ = \frac{c}{\eta_+}$. The time required to traverse a thickness t is $\frac{t}{V_+} = \frac{t\eta_+}{c}$. The frequency of the rotation is ν and the number of rotations occuring in the time $\frac{t}{V_+}$ is simply the frequency multiplied by the time. The rotation in degrees for the positive component is thus $360 \left(\frac{c}{\lambda}\right)\left(\frac{t\eta_+}{c}\right) = 360 \left(\frac{t\eta_+}{\lambda}\right)$

A similar line of reasoning would give the rotation for the negative component as $360 \left(\frac{t\eta_-}{\lambda}\right)$. The net rotation is equal to one half of the difference of these two values

$$\theta = \frac{1}{2} \left(\frac{360\ t}{\lambda}\right) (\eta_- - \eta_+)$$

Expressed in radians

$$\theta = \frac{t\pi}{\lambda} (\eta_- - \eta_+)$$

A P P E N D I X B

Knowing that $(\eta_{\pm} - i\kappa_{\pm})^2 = 1 - \frac{Ne^2/(m^*\omega\varepsilon_o)}{(-\omega \pm \omega_c \pm ig)}$ and that

$\theta = \frac{\omega t}{4\eta c}(\eta_-^2 - \eta_+^2)$ we can show that $\theta = \frac{BNe^3 t}{2\eta c\varepsilon_o m^{*2} i c \omega^2}$

the following conditions are applied: $\eta_{\pm}^2 >> \kappa_{\pm}^2$, $\omega^2 >> \omega_c^2$, $\omega^2 >> g^2$ where $g = \left(\frac{1}{\tau}\right)^2$ where τ is the relaxation time.

$$(\eta_{\pm} - i\kappa_{\pm})^2 = 1 - \frac{Ne^2/(m^*\omega\varepsilon_o)}{(-\omega \pm \omega_c \pm ig)}$$

Taking the real part and if $\eta_{\pm}^2 >> \kappa_{\pm}^2$ then

$$\eta_+^2 = 1 - \frac{Ne^2}{m^*\omega\varepsilon_o}\left(\frac{-\omega + \omega_c}{(-\omega + \omega_c)^2 + g^2}\right)$$

$$\eta_-^2 = 1 - \frac{Ne^2}{m^*\omega\varepsilon_o}\left(\frac{-\omega - \omega_c}{(-\omega - \omega_c)^2 + g^2}\right) \qquad \omega^2 >> g^2,\ \omega^2 >> \omega_c^2$$

$$\eta_-^2 - \eta_+^2 = \frac{Ne^2}{m^*\omega\varepsilon_o}\left\{\frac{\omega + \omega_c}{\omega^2 + 2\omega\omega_c} + \frac{\omega_c - \omega}{\omega^2 - 2\omega\omega_c}\right\}$$

$\eta_-^2 - \eta_+^2 = \frac{Ne^2}{m^*\varepsilon_o}\left(\frac{2eB}{m^*\omega^3}\right)$, substitute this value in to the expression for the rotation and we obtain

$$\theta = \frac{BN\, e^3 t}{2\eta c\varepsilon_o m^* i c\ \omega^2}$$

REFERENCES

B1 "Biography of Physics" Gamow (Harper). 1961.

B2 "Band Structure Spectroscopy of Metals and Alloys" (Academic Press). 1973.

C1 "Compound Semiconductors" (Reinhold). 1962

E1 "Electronics of Solids" Beam (McGraw-Hill). 1965

I1 "Introduction to Solid State Physics" Kittel (Wiley) 1971

O1 "Optics" Fincham, Freeman (Butterworth). 1974

O2 "Optical Properties of Solids" Smith (Plenum Press). 1969

P1 "Physics of Solids" Wert and Thompson (McGraw-Hill). 1970

P2 "Physics of Solid State Electronics" Shive (Merrill).

P3 "Physical Optics" R.W. Wood (MacMillan). 1919

P4 "Principles of Electrodynamics" Aleksey, Matveyev (Reinhold). 1966.

P5 C.R. Pidgeon, Ph.D. Thesis, Reading, England.

R1 S. Rosenbaum, Ph.D. Thesis, University of Ottawa. 1972.

S1 "Semiconductors and Semimetals" Vol. 8, Willardson and Beer (Academic Press). 1972

T1 E. van Tongerloo, Ph.D. Thesis, University of Ottawa. 1969.

1925 B1 Bridgman Proc. Am. Acad. Arts. Sci. 60 305.

1928 B1 F. Bloch Z. Physik 52 555.

1934 J1 Jones, Zener Proc. Roy. Soc. A 145 268.

1952 W1 H. Welker Z. Naturforsch 7a 744.

1954 A1 Abeles Meiboom Phys. Rev 95 #1 31.

1956 K1 Kane J. Phys. Chem. Solids 1 83.

W1 H. Welker, Weiss Solid State Physics 3 65.

W2 H. Welker, Weiss Solid State Physics 3 1.

1957 K1 Kane J. Phys. Chem. Solids 2 131.

E1 Ehrenreich J. Phys. Chem. Solids 2 131.

1958 S1 Stephen, Lidiard J. Phys. Chem. Solids 9 43.

P1 Pauw, Van der Philips Res. Rep. Vol. 13 No. 1.

1959 S1 Smith, Moss, Taylor Phys. Chem. Solids 11 131.

1962 S1 Smith Pidgeon Prosser, Proc. Inter. Conf. on Semiconductor Physics, Exeter p. 301.

1966 T1 E. H. van Tongerloo, Woolley Can. J. Phys. 46 1199.

1967 G1 Clarke, Holonyak Phys. Rev. 156 913.

1969 A1 Aubin, Woolley Can. J. Phys. 46 1191.

A2 Aubin, Thomas, van Tongerloo, Woolley Can. J. Physics 47 631.

1971 T1 Thomas, Wooley Can. J. Phys. 49 2052.

1973 B1 Berolo, Woolley, Van Vechten Phys. Rev. B 8 8.

G1 Gratton, Woolley J. Elec. Mat. 2 #3 455.